High spatial resolution WRF-Chem model over Asia: Physics and chemistry evaluation

Pierre Sicard, Paola Crippa, Alessandra de Marco, Stefano Castruccio, Paolo Giani, Juan Cuesta, Elena Paoletti, Zhaozhong Feng, Alessandro Anav

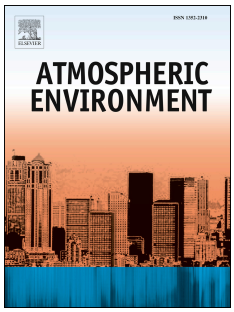

High spatial resolution WRF-Chem model over Asia: Physics and chemistry evaluation

Pierre Sicard, Paola Crippa, Alessandra De Marco, Stefano Castruccio, Paolo Giani, Juan Cuesta, Elena Paoletti, Zhaozhong Feng, Alessandro Anav

PII: S1352-2310(20)30737-8

DOI: https://doi.org/10.1016/j.atmosenv.2020.118004

Reference: AEA 118004

To appear in: *Atmospheric Environment*

Received Date: 2 June 2020

Revised Date: 10 October 2020

Accepted Date: 12 October 2020

Please cite this article as: Sicard, P., Crippa, P., De Marco, A., Castruccio, S., Giani, P., Cuesta, J., Paoletti, E., Feng, Z., Anav, A., High spatial resolution WRF-Chem model over Asia: Physics and chemistry evaluation, *Atmospheric Environment* (2020), doi: https://doi.org/10.1016/j.atmosenv.2020.118004.

Author contribution. P.S., A.A. and A.D.M. conceived the project. A.A., P.C., S.C., P.G. and J.C. carried out modelling. A.A., P.S., Z.Z., E.P. and A.D.M. analyzed the modelling outputs. All authors participated in writing of the manuscript, in particular P.S. and A.A.

High Spatial Resolution WRF-Chem Model over Asia: Physics and Chemistry Evaluation

Pierre Sicard[(1)*], Paola Crippa[(2)], Alessandra De Marco[(3)], Stefano Castruccio[(4)], Paolo Giani[(2)], Juan Cuesta[(5)], Elena Paoletti[(6)], Zhaozhong Feng[(7)], Alessandro Anav[(3)]

[(1)] ARGANS, Sophia Antipolis, France; [(2)] Department of Civil and Environmental Engineering and Geosciences, University of Notre Dame, USA; [(3)] Italian National Agency for New Technologies, Energy and the Environment, C.R. Casaccia, S. Maria di Galeria, Italy; [(4)] Department of Applied and Computational Mathematics and Statistics, University of Notre Dame, USA [(5)] Laboratoire Inter-universitaire des Systèmes Atmosphériques (LISA), UMR7583, Université Paris-Est Créteil et Université de Paris, CNRS, Créteil, France; [(6)] National Research Council, Sesto Fiorentino, Italy; [(7)] School of Applied Meteorology, Nanjing University of Information Science and Technology, Nanjing 210044, China.

Abstract

The representation of air quality and meteorology over Asia remains challenging for chemical transport models as a result of the complex interactions between the East Asian monsoons and the large uncertainty (in space and time) of the high anthropogenic emissions levels over the region. High spatial resolution models allow resolving small-scale features induced by the complex topography of this region. In this study, the Weather Research and Forecasting model with Chemistry (WRF-Chem) was used to simulate the spatial and seasonal variability of main physical and chemical variables over Asia for the year 2015 at 8-km horizontal resolution to enable resolving small-scale features induced by the region complex topography. The simulated atmospheric composition was evaluated against satellite retrievals (MOPITT, IASI+GOME2, MODIS and OMI) in addition to ground-based observations in China for the year 2015, while the meteorological variables were evaluated by several observational-based datasets (ERA5, CRU, MODIS, MTE). Results showed low to moderate seasonal biases for major meteorological variables, i.e. air temperature, relative humidity, precipitation, latent heat, sensible heat and snow cover fraction. Overall, WRF-Chem reproduced well the spatial and seasonal variability of lowermost tropospheric ozone content, total column carbon monoxide and aerosol optical depth, while large discrepancies were found for tropospheric nitrogen dioxide content, mainly during the warm season. In consistency with previous studies, the different biases between model-simulated and satellite-retrieved values can be mainly attributed to i) the large uncertainties in anthropogenic and natural nitrogen oxides emission estimates, as well as dust and sea salt emissions in the case of aerosol optical depth, and ii) some coarse parameterizations used to reproduce main small-scale features (e.g. meteorology, chemical processes, dry deposition to vegetation). Compared to ground-based observations, the WRF-Chem model reproduced well the mean annual cycle of surface nitrogen dioxide, ozone and fine particles concentrations in all seasons across China. Our results suggest that WRF-Chem provides reliable spatio-temporal patterns for most of the meteorological and chemical variables, adding thus confidence to its applicability in the context of air pollution risk assessment to human and ecosystems health.

Keywords: Asia, satellite, regional climate model, remote sensing, WRF-Chem

***Corresponding author**: psicard@argans.eu

1. Introduction

China and India are the two most populous countries of the world (~ 2.8 billion people) and have experienced a rapid growth in industrial, transportation, urbanization and agricultural activities in recent years (Kumar et al., 2015; Zhang et al., 2016a). This explosive economic growth has significantly increased anthropogenic emissions of several trace gases and aerosols over Asia in the last decades (Kumar et al., 2015; Zhang et al., 2016b; Lefohn et al., 2017), with China becoming the largest emitter of air pollutants worldwide (Liu et al., 2015; Quéré et al., 2015; Boden et al 2017; Wang et al., 2017a).

The increasing air pollution levels pose health risks to billions of people (Zhong et al., 2016): in fact, in major metropolitan agglomerations across Asia (e.g. Bangladesh, China, India and Nepal) surface ozone (O_3) concentrations regularly exceed the ambient air quality standard of 100 ppb as hourly value (Wang et al., 2017a), while annual $PM_{2.5}$ concentrations exceed 100 $\mu g\ m^{-3}$ (Zhang and Cao, 2015; Venkataraman et al., 2018). These high levels of air pollutants produce acute and chronic effects on population including premature mortality due to cancer, respiratory and cardio-vascular diseases (Lelieveld et al., 2015; Liu et al., 2016; Cohen et al. 2017; Krishna et al., 2017; Burnett et al., 2018) and reduced life expectancy (Apte et al., 2018). In addition, forests and crops are remarkably affected by high pollution levels: in particular, effects on plants include, among others, yield (Tang et al., 2013; Tai et al., 2014; Sicard et al., 2016a; Tian et al., 2016; Feng et al., 2019) and biomass decline (Wittig et al., 2009; Feng et al., 2015; Li et al., 2017). Krishna et al. (2017) estimated that air pollution contributes to 13-22% of all deaths in South Asia. Other studies showed that for the year 2015 air pollution led to 4.5 million premature deaths and more than half occurring in China and India (Landrigan et al., 2017; Giani et al., 2020), with fine particulate matters ($PM_{2.5}$) causing around 1 million premature deaths every year (Cohen et al., 2017; Li et al., 2018; Burnett et al., 2018).

For these reasons, monitoring of air quality plays a pivotal role to preserve human and ecosystem health; in this regard, in 2013, the State Council of China issued the Air Pollution Prevention and Control Action Plan (Wang et al., 2018), while India introduced policies and National Clean Air Programme (Sagar et al., 2016) to provide a framework for air quality monitoring in order to mitigate the air pollution and attain air quality standards (Sagar et al., 2016; Goldemberg et al., 2018; Wang et al., 2018). In addition to surface measurements, chemical transport models (CTMs) represent a valuable tool to predict formation/removal of air pollutants and their transport, and provide air quality information over remote regions or scarcely populated areas where measurements are not available (Sicard et al., 2017). However, before providing any assessment of impact of air pollution on human and vegetation health, it is mandatory assessing how well models perform in reproducing the spatio-temporal variability of both physical and chemical variables.

In general, regional CTMs have been found able to reproduce observed spatial pattern of air pollutants and their seasonal changes (Spiridonov et al., 2019; Li et al., 2018; Liu et al., 2018) in both North America and Europe (discussed below). However, regional chemistry models still reproduce poorly the observed spatial pattern of main air pollutants over the Asian region because of (i) complex landscape ranging from high elevations of Himalayan plateau to megacities of Easter China; (ii) large uncertainties in removal of trace gases through dry deposition to vegetation associated to a mosaic land cover (Monks et al., 2015), ranging from tropical rainforest to boreal forest and semi-arid or desert area; (iii) widely-varying climate system characterized by a summer monsoon system and (iv) large uncertainties in

anthropogenic emissions (e.g. Amnuaylojaroen et al., 2014; Jena et al., 2015). Consequently, remote sensing data represent a unique opportunity to evaluate the spatio-temporal distribution of air pollutants simulated by regional CTMs (Tuccella et al., 2012; Crippa et al., 2016, 2017; Georgiou et al., 2018; Crippa et al., 2019). China adopted in 2012 the Ambient Air Quality Standard for human health protection, and started reporting hourly observations of main air pollutants from about 1,500 monitoring stations at countrywide (MEP, 2012). These monitoring stations offers an unprecedented way to evaluate model-simulated surface concentrations of air pollutants.

The coupled Weather Research and Forecasting model coupled with Chemistry (WRF-Chem) model is widely used for regional air quality simulation worldwide and validated against ground-based observations, e.g. over North America (McKeen et al., 2005; Chuang et al., 2011; Archer-Nicholls et al., 2014; Yahya et al., 2015; Zhang et al., 2017), Europe (Schürmann et al., 2009; Solazzo et al., 2012; Tuccella et al., 2012; Ritter et al., 2013; Karlický et al., 2017; Werner et al., 2017; Spiridonov et al., 2019; Visser et al., 2019) and South or East Asia (Tie et al., 2007; Kumar et al., 2012a,b; Gao et al., 2014; Zhong et al., 2016; Zhang et al., 2016; Sharma et al., 2017; Li et al., 2018; Xu et al., 2018; Reddington et al., 2019). A few studies reported the WRF-Chem performances over East Asia (Zhang et al., 2016; Zhong et al., 2016) and South Asia (Kumar et al., 2012a,b; Sharma et al., 2017) for air pollutants and meteorology, however the coarse resolution and lack of ground observations limit the model skill to reproduce small-scale processes (e.g. Crippa et al., 2017; Chen et al., 2019). In this regard, the new generation of high spatial resolution reanalysis offers a unique opportunity to run CTMs at very high spatial resolutions over the South-East Asia.

The aim of this paper is to conduct a WRF-Chem simulation of meteorological fields and air pollutants, and evaluate the model performance over a large area covering India and China. The novelty is related to the availability of ground observations in China to validate the WRF-Chem outputs. Therefore, we performed the simulations at fine resolution to allow the model to reproduce well the local variability of climatic and chemical parameters. Despite ground-based observations are amongst the most accurate and reliable datasets to evaluate regional climate models, the lack of spatial representativeness of air quality monitoring stations (Beelen et al., 2009; Sicard et al., 2016b) limits the model evaluation to the regions covered by data. To overcome this gap in spatial heterogeneity, and assess the ability of the WRF-Chem model to reproduce regional patterns of trace gases, we firstly compare simulated data with satellite-based measurements; successively, we use recent ground observations across China to validate surface concentrations of air pollutants.

2. Materials and Methods

2.1. WRF-Chem model

The WRF model is a limited-area, non-hydrostatic, terrain-following eta-coordinate mesoscale model (Skamarock et al., 2008). This model has been further developed to include various gas-phase chemistry and aerosol mechanisms creating the coupled chemistry-climate WRF-Chem model (Grell et al., 2005). The WRF model system offers multiple options for various physical packages (Skamarock et al., 2008). The dynamical core used in this work is the Advanced Research Weather Research and Forecasting model (Tab. 1); we used a single-moment 6-class scheme to resolve the microphysics (Hong et al., 2006) and the Rapid Radiative Transfer Model for GCMs (RRTMG) for the shortwave and longwave radiation (Iacono et al., 2008). Convective precipitation and cumulus parameterization were resolved

with the new Tiedtke scheme (Zhang et al., 2011), the planetary boundary layer computations were performed using the nonlocal K-profile Yongsei University parameterization (Hong et al., 2006), while the exchange of heat, water and momentum between soil-vegetation and atmosphere was simulated by the Unified Noah Land Surface Model (Chen and Dudhia, 2001).

Similarly to physical parameterizations, many different gas phase chemistry and aerosol options are available in WRF-Chem. Gas-phase chemical reactions are calculated using the chemical mechanism MOZART (*Model for OZone And Related chemical Tracers*) (Emmons et al., 2010) whereas for the aerosols, to reduce the computational cost, we used the GOCART (*Global Ozone Chemistry Aerosol Radiation and Transport*) bulk aerosol approach (Chin et al., 2000). This set-up includes 85 gas-phase species, 12 bulk aerosol compounds, 39 photolysis and 157 gas-phase kinetic reactions.

Anthropogenic emissions are based on the EDGAR-HTAP (*Emission Database for Global Atmospheric Research for Hemispheric Transport of Air Pollution*) global emission inventory which includes diurnal cycle of emissions of gaseous pollutants such as SO_2, NO_x, CO, non-methane volatile organic compounds (NMVOCs) and NH_3 as well as black carbon and particulate matter from the following source sectors: aviation, shipping, agriculture, power generation, industrial non-power, land transport and residential energy use (Janssens-Maenhout et al., 2015). This dataset is available at 0.1°×0.1° horizontal resolution for the year 2010, with no year adjustments. Fire emissions are provided using the FINN (Fire INventory from NCAR) inventory (Wiedinmyer et al., 2011). This dataset provides estimates of trace gases and particles emitted by open biomass burning at ~1 km resolution (Wiedinmyer et al., 2011). Biogenic emissions are calculated online using the MEGAN (Model of Emissions of Gases and Aerosols from Nature) model (Guenther et al. 2012), dust emissions are estimated online using the GOCART model (Ginoux et al., 2001), whereas sea-salt emissions are calculated using the method by Gong (2003). Anthropogenic dust emissions (e.g. re-suspended road dust) are not included.

In addition, MOZART-4/Goddard Earth Observing System Model version 5 (GEOS-5) data were used for chemical and aerosol boundary conditions. The MOZART-4 data is a model outputs dataset available at a horizontal grid resolution of 1.9°×2.5° every 6 h and is driven by the National Aeronautics and Space Administration (NASA). The initial and boundary meteorological conditions (including time varying sea surface temperature), required to run the model, are provided by the European Centre for Medium-range Weather Forecast (ECMWF) re-analysis project ERA5, with a horizontal resolution of about 31 km every 3 hours.

In this study we used WRF-Chem (v3.9) to simulate meteorology and air quality from 20th December 2014 to 31st December 2015 using the first 10 days as spin up. We conducted a fully free running simulation (i.e. without nudging) for the entire year 2015. The model domain is projected on a Lambert conformal grid (780 x 690 grid cells) with a horizontal grid resolution of 8 km with 30 vertical levels extending from the surface up to 50 hPa. A synthesis of parameterizations and input data used in this study is given in Tab. 1.

2.2. Datasets for model evaluation

To evaluate the spatio-temporal patterns of simulated surface air temperature, relative humidity and precipitation, we compared model results against Climatic Research Unit (CRU)

observed data, a monthly high-resolution (0.5°×0.5°) gridded dataset over land areas (Mitchell and Jones, 2005). In addition to CRU, which can be regarded as an independent dataset, for the evaluation of physical variables, we also compared simulated data against the boundary conditions used to drive the model (i.e. ERA5); this allows assessing if a bias has been introduced into the model by its forcing (Mooney et al., 2013) or is mainly due to poor representation of some physical processes within the model (Tang et al., 2017). In addition, in order to remove any possible bias in surface temperature related to the difference in topography between the coarse reference data and the finer model output, we downscaled both CRU and ERA5 temperature to our domain using a dry-adiabatic lapse. Sensible and latent heat fluxes were evaluated using the Machine Tree Ensemble (MTE) a 0.5° × 0.5° gridded dataset (Jung et al., 2011) created by upscaling eddy covariance measurements collected around the world (Jung et al. 2009, 2011). This dataset has been widely employed to evaluate the performances of land surface models, including NOAH-MP, a land surface scheme often used within WRF (Ma et al., 2017). We used the Moderate Resolution Imaging Spectro-radiometer (MODIS) product from the NASA Terra Satellite to evaluate the snow cover fraction (Hall et al., 2010); this dataset provides monthly data with a resolution of 0.05° x 0.05° (Hall and Riggs, 2015).

We have evaluated the WRF-Chem simulations of NO_2 concentrations against satellite retrievals from the Ozone Monitoring Instrument (OMI), flying aboard NASA's EOS-Aura satellite. This instrument measures the radiation backscattered by the Earth's atmosphere and surface, and provides the daily global retrievals of several trace species and aerosols with a spatial resolution of 13 km × 24 km at nadir (Boersma et al., 2011). To evaluate the ability of the model to reproduce reliable spatial and seasonal NO_2 estimates, we compared the tropospheric NO_2 content simulated by WRF-Chem with spatial resolution of OMI data available from KNMI (Royal Netherlands Meteorological Institute). Similarly, the CO amounts derived from the Measurement of Pollution in the Troposphere (MOPITT), flying aboard the NASA EOS-Terra satellite, are compared with WRF-Chem. MOPITT measures the thermal infrared (IR) radiation with a spatial resolution of about 22 km x 22 km; these radiances are then used to retrieve CO mixing ratios profile and total column amounts (Deeter et al., 2003). Here we used version 6 Level 3 MOPITT CO data from the thermal infrared band (TIR) to evaluate the spatio-temporal patterns of total column content simulated by the model.

Tropospheric O_3 distributions simulated by WRF-Chem were compared to those derived from the IASI-GOME2 multispectral approach, combining Infrared Atmospheric Sounding Interferometer observations in the IR and Global Ozone Monitoring Experiment-2 measurements in the Ultraviolet (Cuesta et al., 2013, 2018). IASI-GOME2 has allowed the first satellite observation of the horizontal distribution of O_3 pollution plumes located below 3 km of altitude, and also quantified the photochemical production of lowermost tropospheric (LMT) O_3 across East Asia. This method is based on measurements from two instruments onboard the MetOp satellite series since 2006 that offer global coverage every day with a relatively fine ground resolution (12 km x 25 km for IASI at nadir and 80 km x 40 km for GOME-2). In this analysis, we have evaluated the LMT O_3 content integrating between the surface and 3km height.

For the evaluation of aerosols simulations, we used aerosol optical depth (AOD) data at a wavelength of 550 nm derived from the MODIS instruments onboard the Terra and Aqua satellites. Level-2 MODIS Collection-6 data have a resolution of 10 × 10 km (at nadir). In this analysis, we used the extinction coefficients simulated by WRF-Chem and extracted daily at the satellite overpass time.

In our evaluation, we accounted for the satellite retrieval sensitivity by smoothing WRF vertical profiles with satellite averaging kernels (Kumar et al., 2012a). In the case of O_3, the IASI+GOME2 averaging kernel $A_{IASI+GOME2}$ and *a priori* O_3 profiles $X_{apriori}$ used by IASI+GOME2 were then applied to the WRF-Chem O_3 profile X_{int} (interpolated over the IASI+GOME2 vertical grid) to obtain smoothed WRF-Chem O_3 profile accounting for the satellite retrieval sensitivity, as classically done with the equation:

$$X_{WRF\text{-}Chem\ (O3)}^{smoothed} = X_{apriori} + A_{IASI+GOME2}\,[X_{int} - X_{apriori}] \quad (1)$$

A similar procedure was used to transform the modeled CO profiles using MOPITT averaging kernels and a priori profiles (Kumar et al., 2012a). For transforming the WRF-Chem simulated tropospheric NO_2 content for comparison to OMI retrievals, the procedure requires the user to calculate the transformed model profile (Y_{trop}) as:

$$Y_{trop} = A \times \frac{AMF}{AMF_{trop}} \times X_{trop} \quad (2)$$

where A is the total column averaging kernel, AMF and AMF_{trop} are the air mass factors for the total columns and tropospheric columns, respectively, and X_{trop} is the tropospheric vertical profiles of NO_2, simulated by WRF-Chem, interpolated to the OMI pressure grid (Kumar et al., 2012a).

Finally, hourly NO_2, O_3, $PM_{2.5}$ and PM_{10} in-situ measurements were collected from 1497 air quality monitoring stations across China (589 rural and 908 urban), after checking for data quality. A minimum data capture of 75% was imposed to calculate seasonal mean concentrations.

2.3. **Assessment of model performance**

The model performance was evaluated over different seasons (January-February-March, JFM; April-May-June, AMJ; July-August-September, JAS; October-November-December, OND) by using the Pearson's correlation coefficient (r), mean bias (MB) and the fractional bias (FB). The first metric allows estimating the correlation pattern, thus the spatial agreement between model and observations. For physical parameters, the MB provides the absolute bias of the model, with negative and positive values indicating respectively underestimation and overestimation by the model while the FB (in %) is used for the chemical variables, as in this case the absolute bias would be hard to interpret. The mean biases were computed pointwise and then averaged over the whole domain:

$$MB^j = \frac{1}{N_{obs}^j} \sum_{i=1}^{N_{obs}^j} \left(Mod_i^j - Obs_i^j\right) \quad (3)$$

$$FB^j = \frac{1}{N_{obs}^j} \left[\frac{\sum_{i=1}^{N_{obs}^j} (Mod_i^j - Obs_i^j)}{\sum_{i=1}^{N_{obs}^j} \left(\frac{Mod_i^j + Obs_i^j}{2}\right)} \right] \times 100 \quad (4)$$

with Obs^i_j and Mod^i_j the observed and modeled values and N^j_{obs} the number of data at time i and station j over the domain. These metrics were successfully used in several studies for evaluating the performance of regional air quality models (e.g. Savage et al., 2013; Pope et al., 2015; Im et al., 2015; Crippa et al., 2016; Ghim et al., 2017; Crippa et al., 2019).

In case of in-situ data, we extracted WRF-Chem results at the lowest model layer and, for each station, we calculate the Pearson's correlation coefficient to assess the ability of the

model to reproduce the mean annual cycle and the mean bias to provide a measure model's error; in the following analysis results are presented as an average over all the stations.

3. Results

3.1. Evaluation of meteorological variables

The general ability of the WRF model to reproduce realistic spatio-temporal patterns of most relevant physical and chemical variables is assessed by comparing simulated output with observational data averaged over different seasons for the reference year 2015. Looking at the surface air temperature, WRF well captures the observed spatial pattern with a decreasing south-north gradient and a cold area over the Tibetan plateau. In general, the spatial distribution of 2-m temperature during all the seasons was very similar to ERA5 and only slightly different from CRU (Fig. 1). The largest bias was observed during JFM, where the model was warmer than the reference data over the northern part of the domain and colder in most of western China, Vietnam, Laos, and Thailand (Fig. 1). In addition, large discrepancies were observed over the Tibetan plateau, where the coarse resolution of the datasets and the sparse availability of local measurements could explain the mismatch. The large thermal heating occurring over the Indian region during spring and early summer (AMJ) is well captured by the model, which is a pre-requisite to correctly simulate the summer Asian monsoon. The high agreement in the spatial pattern is confirmed by the high spatial correlation ranging between 0.98 and 0.99 with respect to both ERA5 and CRU datasets, while the MB ranged from - 1.51°C in winter (JFM) to 0.07°C in summer (JAS) using ERA5 as reference, and from - 1.82°C in winter to - 0.20°C in summer when compared to CRU (Tab. 2).

Unlike seasonal variations in surface air temperature, which are mainly determined by the insolation patterns, seasonal precipitation variations are strongly influenced by vertical movement of air due to atmospheric instabilities of various kinds and by the flow of air over orographic features; thus, to simulate accurately the seasonally varying pattern of precipitation, models must correctly simulate a number of processes (e.g., evapotranspiration, condensation, and transport) (Randal et al., 2007). The spatial distribution of seasonal mean precipitation from model and reference data (ERA5 and CRU) is depicted in Fig 2. In general, the model was able to capture the major convective centers as in the observations. WRF overestimated the precipitation over the Himalayan region in JFM and over eastern China in AMJ, nevertheless, it is important to note that WRF resolved the finer details of orographic precipitation along the Himalayan foothills, which were missing both in ERA5 because of its coarser resolution and in CRU due to the lack of widespread measurement stations. Besides, WRF well reproduced the main monsoon features. The relevant thermal heating occurring during AMJ over the Indian peninsula results in a pressure gradient with lows over the landmasses and highs over the colder ocean, which causes a strong moisture advection from the Bay of Bengal to Indian Peninsula leading to increased precipitation over South-East Asia and the Indian landmass region during JAS. Looking at the spatial agreement, except for CRU in winter ($r = 0.73$), the correlation coefficient exceeded 0.80 during all the seasons and for both the datasets. The area averaged bias, with respect to the CRU observation, was 0.21-0.25 mm/day during the cold periods (OND-JFM) and 0.68-0.74 mm/day during the warm periods (AMJ-JAS), while compared to ERA5, WRF showed a slight wet bias during the warm periods (+ 0.15-0.27 mm/day) and a slight dry bias (about - 0.05 mm/day) during the cold seasons (Tab. 2). Large discrepancies (overestimation) were observed between 2-m relative humidity and CRU observations over central Asia, Western China and India (Fig. 3) while an

underestimation was observed over the western part of the domain compared to ERA5 during JAS and OND. The spatial correlation ranged from 0.95 to 0.99 for both ERA5 and CRU datasets. The WRF model underestimated the relative humidity with respect to ERA5 during all the year, from - 1.5% in JFM to - 4.5% in JAS, and an overestimation was observed compared to CRU dataset, in particular during the warm period with a MB of 11-12%.

Looking at latent heat we found an overall good agreement between the WRF model and the reference datasets (Fig. 4), with spatial correlation exceeding 0.92 for both datasets (Tab. 2). Nevertheless, WRF remarkably overestimated surface latent heat during the warm seasons, especially over South and Southeastern Asia, with the largest bias found in JAS and ranging between 2.6 W/m² and 13.2 W/m² compared to ERA5 and MTE, respectively. This overestimation was strictly related with the slight overestimation of rainfall during the same season which brings more water on the land surface that can re-evaporate, subsequently amplifying convective precipitation. Similarly, the sensible heat was well simulated with a spatial correlation ranging from 0.82 in JFM for MTE dataset to 0.94 in AMJ for ERA5. Compared to ERA5, WRF model overestimated the sensible heat during the warm period (16.4-19.4 W/m²), in particular over the Western part of the domain, while a lower overestimation is reported for MTE (7.9-11.5 W/m²) over the same season. In contrast during JFM and OND, WRF model well reproduced the observed spatial patterns (Fig. 5) with a slight underestimation in winter (- 1.2 and - 2.8 W/m²).

Besides, WRF well reproduced the snow cover fraction, with a spatial agreement ranging from 0.74-0.77 in summer to 0.92-0.95 in winter for ERA5 and MODIS datasets, respectively (Tab. 2). Compared to MODIS data, WRF slightly overestimated the snow cover fraction in JFM (0.6%) and AMJ (0.2%) mainly around the Tibetan plateau and underestimated it in JAS (about - 0.1%) and OND (- 1.7%), WRF underestimated the snow cover throughout the year when compared to ERA5, with a mean bias ranging from - 0.9% in JAS to - 3.2% in AMJ. The main discrepancies were observed over North Siberia in JFM, over the Tibetan plateau in AMJ and over both areas in OND (Fig. 6).

3.2. Evaluation of chemical variables

The spatial distributions of model-simulated and OMI-retrieved seasonal mean tropospheric NO_2 content during winter, spring, summer and autumn for the year 2015 are shown in Fig. 7. Both WRF-Chem and OMI showed, during all the seasons, the highest tropospheric NO_2 content over the polluted region around Beijing and over Korean peninsula, followed by the Indo-Gangetic Plain region, with hot spots located in correspondence of large urbanized areas such as Seoul (South Korea) and New Delhi (India). The lowest values were found above the Tibetan plateau. The spatial correlation averaged over the entire domain ranged between a 0.89 in AMJ and 0.91 in JFM. The percentage differences between WRF-Chem and OMI tropospheric NO_2 content showed a slight underestimation of the model by 2-8% during the cold period (Tab. 3) while the concentrations of NO_2 were significantly under-predicted by WRF-Chem during the warm period (64-70% in AMJ-JAS). Conversely, large overestimations occurred during the cold months (JFM and OND), mostly over polluted regions (e.g. Eastern China). The positive and negative biases found in summer and winter, respectively, compensated with each other and led to an overall small FB (- 2%).

The highest total column CO was observed over the Southeastern and Eastern Asia and the lowest column CO values were found above the Tibetan plateau (Fig. 8). The simulated total CO column showed a high spatial correlation coefficient (about 0.97) during all the seasons (Tab. 3). The model performed well for simulating CO with a FB < ± 10% of MOPITT. The

agreement between WRF-Chem and MOPITT is higher in autumn (FB: + 3%) than in spring (FB: + 7%) and summer (FB: + 8%). The simulated total column CO was slightly underestimated over Eastern Asia during all seasons and over Southeastern Asia in winter and autumn. In summer, the most important overestimation was observed over Southeastern Asia and India (Fig. 8).

The spatial and seasonal distributions of model-simulated and IASI+GOME2-retrieved LMT O_3 content (integrated up to 3km height) are shown in Fig. 9. The WRF-Chem model simulated well the spatial distributions and the seasonal variations of O_3. A particular good spatial agreement is remarked for the summer season, with a spatial correlation of 0.99 (Tab. 3). During spring and winter, the spatial agreement is moderate (r = 0.61 and r = 0.76, respectively), while it is fairly low in winter (r = 0.43). The highest O_3 content was similarly depicted in Eastern Asia and in the latitude band 20-45°N, in particular over the Indo-Gangetic Plain region, in both datasets. Although overestimated in the cold seasons, WRF-Chem simulates correctly the eastward export of tropospheric O_3 over the Yellow and Japan Sea (30-40°N 120-130°E). Model and satellite data also agree to show very low LMT O_3 values above the Tibetan plateau during the cold season and below 30°N latitude in summer. North of these high mountains (40°N 80-100°E), high abundances of O_3 during summer and spring depicted by IASI+GOME2 are consistently simulated by WRF-Chem. The overall seasonal cycle is consistently shown by both datasets, with highest concentrations in spring, a little lower in summer and lowest in autumn. The FB over the model domain exhibited a seasonal variability with limited overestimation during the warm season (3-7% in spring and summer), in the 20-30°N latitude band, and larger over-prediction (11-13%) during the cold period (winter and autumn). In addition, we remark that only IASI+GOME2 retrievals show moderate enhancement of O_3 concentrations north of 45°N during winter, probably associated with downward transport of O_3 from both upper troposphere and stratosphere. This difference between IASI+GOME2 and model data was also remarked in a comparison with respect to other simulations performed with WRF-Chem in springtime 2009 over East Asia (Cuesta et al., 2018).

Looking at the aerosol optical depth (Fig. 10), both WRF-Chem and MODIS showed, during all the seasons, the highest AOD over the polluted region of Eastern Asia, over the Goby desert and over the Indo-Gangetic Plain region. The spatial correlation ranged between 0.86 in summer and 0.93 in winter (Tab. 3). The model-simulated AOD were lower than those from MODIS with a FB of - 19% and - 2% for JFM and OND, respectively, in particular over the polluted region of Eastern China and Indo-Gangetic Plain region (Fig. 10). WRF-Chem overestimated the AOD by 6% and 20% in spring and summer over Southern part of the domain.

Compared to in-situ measurements, WRF-Chem was able to reproduce the surface NO_2 concentrations over China during all the seasons (Fig 11). The high concentrations over polluted regions are well captured, despite some stations showed a large bias, while minimum NO_2 concentrations, found in Western China, are slightly underestimated. Overall, the correlation coefficient computed from mean daily concentrations was 0.29, with a mean bias of 10.1 ppb and a FB ranging from 35% in spring to 45% in autumn (Tab. 4). These statistics were calculated from the mean of the metrics computed over the stations, thus stations with poor agreement significantly contribute to lower model skills. As poor model performances were expected, particularly in urban areas, where a regional chemistry transport model is unable to correctly predict the observed hourly variability of air pollutants concentrations, which depends on local processes, we also computed the correlation comparing the mean temporal evolutions averaged over all the stations. In this latter case, the model performance

was remarkably better, with a temporal correlation of 0.71 (data not shown). Unlike NO_2, the comparison of surface O_3 showed a complex bias pattern: the model well reproduced O_3 during cold seasons (FB = - 8% in JFM, - 15% in OND), in particular concentrations below 15 ppb over megacities (Fig. 12). Similarly, high O_3 concentrations over Tibetan plateau are well represented during all the seasons. Nevertheless, during warmer months (AMJ and JAS), the WRF-Chem systematically overestimated surface O_3 concentrations (FB = 23-24%). The mean annual cycle of O_3 is slightly better simulated compared to NO_2, with a correlation coefficient of 0.51 (0.90 in case of correlation computed from the mean temporal evolution averaged over all the stations), while the mean bias was 5 ppb (Tab. 4). Looking at surface $PM_{2.5}$ (Fig. 13) and PM_{10} (Fig. 14) concentrations during the cold period, the high concentrations (exceeding 100 µg m^{-3}) over polluted regions and megacities in Eastern China are well captured (FB = 5% in JFM for both $PM_{2.5}$ and PM_{10}), while low $PM_{2.5}$ and PM_{10} concentrations in Western China (less than 10 µg m^{-3}) are slightly overestimated. During the warm period, the surface concentrations are well captured across China, with a slight overestimation in AMJ for PM_{10} (FB = 11%). The highest overestimation is observed in summer with a FB of 29% and 36% for PM_{10} and $PM_{2.5}$, respectively (Tab. 4). Overall, the correlation coefficient computed from mean daily concentrations was 0.44 for $PM_{2.5}$ and 0.35 for PM_{10}, with a mean bias of 10.4 µg m^{-3} and 14.8 µg m^{-3}, respectively (Tab. 4). By considering the mean temporal evolutions averaged over all the stations, the temporal correlations were 0.83 and 0.71, respectively (data not shown).

4. Discussion

Capturing spatiotemporal patterns of trace gases and weather patterns over Asia is challenging for chemistry transport models because of the complex orography associated to the monsoon systems and large uncertainty in the anthropogenic emission inventories over heavily populated regions in Asia (Kumar et al., 2015; Zhang et al., 2016a). In this study, the WRF-Chem model was used to simulate the spatial and seasonal variability of main physical and chemical variables over the Asian region at fine horizontal resolution (8 km) to capture local small-scale processes.

In addition to surface air temperature and moist fluxes, which influence the rate of chemical reactions close to land surface and the removal of air pollutants through wet deposition, respectively, heat fluxes also play a pivotal role in surface energy balance and influence the Asian monsoon (Wang et al., 2014, 2016, 2017b). When compared to ERA5 and CRU datasets, WRF well reproduced meteorological observational-based data. In particular, looking at temperature, WRF performed well in terms of spatial distributions over time, even over complex terrain with uneven surface topography, such as Tibetan plateau and Himalayan chain. To reproduce observed patterns over Tibetan plateau, a meteorological model must correctly reproduce several processes ranging from convection to thermal balance. Considering the relative humidity, we found slight discrepancies over the Tibetan plateau, particularly in winter, while we found a large bias for surface sensible heat over the Western part of the domain during the warm period. Besides, WRF slightly overestimated the precipitation, in particular during the monsoon period; previous studies suggested that the magnitude of precipitation bias depends on the cumulus parameterization schemes (Ratna et al., 2014; Juneng et al., 2016). The WRF model predicted much stronger rain over Western China, Northern Bay of Bengal and Eastern India. Zhang et al. (2016a) showed that the rainfall overestimation can be attributed to the slightly excessive precipitation predicted by the cumulus Tiedtke scheme, and the apparent underestimation of air temperature is most likely caused by an error in the radiation balance and certain limitations in the Yonsei

University Scheme used in resolving main features of the Planetary Boundary Layer meteorology, particularly over complex terrain such as mountainous regions over high-elevation Tibetan plateau, Vietnam and Laos (Zhang et al., 2016b).

A previous study performed with WRF over South Asia at 45 km of spatial resolution, indicated that the MB was 1-4 °K for temperature, 20-65 % for water vapor and within ± 10 mm/day for the precipitation during all seasons except in summer, with an overestimation exceeding 20 mm/day over Himalaya and along the coastline in Eastern India (Kumar et al., 2012b). In another study where WRF was run over East Asia at 36 km of horizontal resolution, Zhang et al. (2016b) showed a MB ranging from - 1.0°C to + 1.5°C for surface air temperature and moderate to large biases for precipitation (+ 0.2 to + 1.7 mm/day) and relative humidity (+ 0.4% to + 23.4%). In a different study over East Asia, where WRF was run at 50 km of horizontal resolution, using a spectral nudging applied to wind direction and speed and air temperature over the time period 1989-2007, Tang et al. (2017) found for the surface air temperature an averaged MB of 1.77 °C (- 8 to + 4 °C) compared to CRU, and of 1.45 mm (- 4 to + 8mm) for precipitation with an overestimation by 2-8 mm/day in tropical regions and an underestimation of 0.5-1.0 mm/day over Southern China.

In our study, the model performances in simulating surface meteorology were better than the other simulations performed over Asian regions with the same model but with a coarser spatial resolution at 36 - 50 km of spatial resolution (e.g. Kumar et al., 2012a,b; Zhang et al., 2016a,b; Tang et al., 2017); this suggests that the finer model resolution (8 km) helps to resolve small-scale features induced by complex topography e.g. in Himalaya or Sichuan region. In general, increasing model resolution has resulted in improved model simulations and predictions for air temperature, relative humidity, precipitation (Malardel et al., 2016; Prodhomme et al., 2016; Zhang et al., 2016c), global energy budget (Vannière et al., 2019) and orographic winds (Roebber et al., 2004). By using the WRF model with horizontal resolutions of 2, 10 and 30 Km, Lin et al. (2018) showed that finer resolutions improved biases over the Tibetan Plateau, in particular for precipitation. A significant difference was observed from 30 to 10 km of horizontal resolution, suggesting that approximately 10 km of horizontal resolution represents a good compromise (Lin et al., 2018).

The WRF-Chem model well reproduced tropospheric NO_2 content, total column CO and LMT O_3 content with a FB within the air quality model performance criteria, except for NO_2 during the warm season. The highest column content for NO_2, CO and O_3 was observed over Southeastern and Eastern Asia due to road traffic, industries, power plants and biomass burning (Streets et al., 2003; Kumar et al., 2012a; Cooper et al., 2014), with 2015 recording the highest fire activity season since 1997 (Huijnen et al., 2016; Mead et al., 2018). In contrast, the column NO_2, CO and O_3 values above regions of high terrain such as the Tibetan plateau were lower than adjacent regions due to the limited depth of the troposphere and fewer emissions (Cooper et al., 2014).

In this study, WRF-Chem captured the seasonal variability of tropospheric NO_2 content values with a summer minimum and a winter maximum. The winter maximum is due to a lower removal rate of NO_2 with OH radicals, compared to summer (Beirle et al., 2003). The large NO_2 overestimation was observed during winter and autumn over polluted regions with abundant anthropogenic NO_x emissions, such as road traffic and power plants as previously reported e.g. in Europe (Barten et al., 2019; Visser et al., 2019). These results are in agreement with prior studies that found WRF-Chem overestimating tropospheric NO_2 content in urban areas such as London, Madrid, Rome and in cities of Eastern Europe by 5-18 % in urban areas (Barten et al., 2019; Visser et al., 2019), despite they adopted a different chemical

mechanism (i.e., CBM-Z). The NO_x emissions from microbial activity and lightning, which were not considered in our emission inventory, are important during summer in rural areas of Southeastern Asia (Kumar et al., 2012a). The largest discrepancies (underestimation) during spring and summer point to uncertainties in biomass burning, lightning and soil emission estimates (Kumar et al., 2012a; Barten et al., 2019) and another plausible reason is the NO_x removal overestimation through the reaction of dinitrogen pentoxide (N_2O_5) to nitric acid in the WRF-Chem chemical mechanism (Yegorova et al., 2011). The discrepancies in NO_x concentrations can be also explained by no year adjustments for EDGAR-HTAP anthropogenic emission data (based on year 2010), in particular in China. Kumar et al. (2012a) showed that the discrepancies in anthropogenic emission estimates were mainly due to uncertainties in the emissions inventory (emission factors and socio-economic parameters). Prior studies have found that, over South Asia, WRF-Chem tends to overestimate NO_2 tropospheric content from OMI retrievals by 10-50% over South Asia and up to 90% over the Indo-Gangetic Plain region during winter (Kumar et al., 2012a) with a correlation coefficient between model and OMI ranging from 0.61 to 0.73 in 2008 (Kumar et al., 2012a). Over East Asia, WRF-Chem underestimated the tropospheric NO_2 content by up to - 30.6% compared to SCIAMACHY data in 2005 (Zhang et al., 2016b). As NO_x emissions display strong spatial variation, we obtained a better spatial representation and simulations of NO_2 levels, by increasing the model grid resolution, compared to previous studies at coarser scale e.g. at 20 km of grid resolution (Schaap et al., 2015; Barten et al., 2019; Visser et al., 2019).

The seasonal variation of the total column CO is well reproduced by WRF-Chem with highest and lowest values during late autumn-winter and summer (monsoon), respectively. In general, both the model and MOPITT were highest during winter, decreased during spring, attained minimum levels during summer and increased again during autumn. MOPITT CO retrievals over South and Southeast Asia were slightly underestimated by WRF-Chem in spring, between March and May, when biomass burning constitutes the major fraction of total CO emissions (Amnuaylojaroen et al., 2019), suggesting that CO emissions from biomass burning is slightly underestimated. Over South Asia, the WRF-Chem model similarly estimated MOPITT column CO retrievals by - 9.0% to + 7.0% during all seasons with a r value from 0.63 to 0.84 for the year 2008 (Kumar et al., 2012a) and by - 24.2% to + 3.9% over East Asia in 2005 (Zhang et al., 2016b). The annual mean contribution of biomass burning to the total CO emissions was around 24% over Asia (Streets et al., 2003). The slight overestimation of CO retrievals during other seasons (low fire activity) indicated that anthropogenic CO emissions are overestimated over this region (Zhang et al., 2016a). A better treatment of biomass burning sources and improved boundary conditions of CO (e.g. for transboundary inputs, in particular from wildfires, biomass burning and transport) are needed to improve the performance of the total column CO.

The seasonality of LMT O_3 content is well reproduced by WRF-Chem by capturing the increase in O_3 burden during the warm season, with a spring maximum (Sicard et al., 2009; Kumar et al., 2012a; Cooper et al., 2014). Eastern China and Northern India are two main pollution sources, emitting significant amounts of NO_x, CO and VOCs (Wang et al., 2010) in winter and autumn (cold period) leading to the highest LMT O_3 in spring and summer (Cooper et al., 2014). Furthermore, the relatively high biogenic NMVOC emissions and active photochemical reactions constitute favorable conditions for O_3 formation in summer (Sicard et al., 2016b). The WRF-Chem overestimation of anthropogenic NO_2 and CO emissions led to a model overestimation of surface O_3 concentrations in winter (13%) and autumn (11%), in particular in South Asia and Eastern China. A previous study employing an offline regional model showed an overestimation of O_3 levels during summer over India (Roy et al., 2008). As

reported here, the regional models generally underestimate mean O_3 concentrations during high O_3 seasons and overestimate mean O_3 concentrations during low O_3 seasons (Fiore et al., 2009; Huang et al., 2017). The differences in anthropogenic NO_x, CO and VOCs inventories are the dominant factors for the discrepancies in simulated O_3 levels, as already reported in China and Southeast Asia (Ma and van Aardenne, 2004; Amnuaylojaroen et al., 2014). The slight mean bias of LMT O_3 for spring 2015 (3%) entails among other the correct representation of the seasonal variations of stratospheric O_3 intrusions to the upper troposphere. The over-prediction of O_3 and under-prediction of NO_2 in all months indicated an insufficient titration of O_3 by NO (Zhang et al., 2016b). In Southern India and Southeastern Asia, below 30°N latitude, the summer is dominated by cloudy conditions and heavy rainfall due to monsoon leading to lower O_3 levels by reducing the photochemical production of O_3 (e.g. Roy et al., 2008; Kumar et al., 2012a). The FB ranged from - 16% to 0% over South Asia in 2008 (Kumar et al., 2012a) with larger differences during spring and early summer, mainly due to additional O_3 precursor sources (e.g. biomass burning).

High AOD were observed over desert regions due to mineral dust (e.g. Goby) and over areas with large anthropogenic aerosol emissions, especially East and South Asia (Shindell et al., 2013). As EDGAR does not provide black and organic carbon and $PM_{2.5}$ emissions, and GOCART does not include secondary organic aerosols or nitrate aerosols, an under-prediction of aerosol burden is observed in Asia, in particular in winter (Zhong et al., 2016; Zhang et al., 2016a; Crippa et al., 2019). The overestimations of AOD over Eastern China, South and Southeastern Asia in spring and summer, were mainly due to over-predictions in PM_{10} concentrations because of dust emissions (Shindell et al., 2013; Zhang et al., 2016a). Over East Asia, the differences between model-simulated and MODIS-based AOD ranged from -38.7% to + 5.6% in 2005 (Zhang et al., 2016b).

Considering the performances of WRF-Chem for reproducing atmospheric chemistry at ground-level, the recommended benchmarks proposed by Morris et al. (2005), Boylan and Russell (2006) and Emery et al. (2017) for the chemical model performance is FB within ± 15% for O_3 and NO_2 if r is greater than 0.5. By comparing the WRF-Chem model outputs with ground-based observations, overall the WRF-Chem model reproduced well the mean annual cycle of surface O_3, $PM_{2.5}$ and PM_{10} mean concentrations at regional scale in 2015, in particular during the cold season. Furthermore, the model well reproduced the NO_2 titration over the polluted Eastern China. The WRF-Chem model overestimated surface O_3 concentrations during the warm period, when plants are active, then a part of the observed bias can be explained by (i) a poor parameterization of dry deposition to vegetation in the Noah Land Surface Model, leading to an underestimation of dry deposition velocities (Wu et al., 2011), then to a reduction of the O_3 removal capacity by plants; and by (ii) the under-prediction of cloud optical depth and overestimation of photolysis rates by WRF (Ryu et al., 2018). However, when the correlations were computed from the average of individual stations, the performances were much poorer. Nevertheless, this result was partially expected being an intrinsic characteristic of regional models. In other words, a regional CTM (even at high spatial resolution) is not able to reproduce well temporal variation of local urban observations because of the lack of detailed local inputs (both emission inventories and removal processes). Besides, it should be noted that WRF-Chem was forced with annual mean anthropogenic emissions, thus it is hard to reproduce the high frequency temporal variability of observations, especially in urban environments which are extremely dynamics and poorly controlled by natural processes.

5. Conclusions

In this study WRF-Chem was applied at high spatial resolution (8-km) over Asia for the year 2015, to allow resolving fine-scale features over complex topography areas (e.g. Indo-Gangetic Plain region). As we did not use nudging, our results enhance the reliability of this study and the ability of the model to capture spatio-temporal variation of physical and chemical variables. Overall model skills in simulating surface meteorological and air quality were higher than those showed in previous studies focusing on the same region where the model was applied at coarser spatial resolution. In this study, the mean bias ranges are lower than Zhang et al. (2016b) e.g. [- 1.51 °C; + 0.07 °C] vs. [- 1.0 °C; + 1.5°C] for air temperature, [- 0.05 mm/day; + 0.27 mm/day] vs. [+ 0.2 mm/day; + 1.7 mm/day] for precipitation; [- 4.5 %; - 1.5 %] vs. [+ 0.4 %; + 23.4%] for relative humidity and [- 7 %; + 8 %] vs. [- 24.2 %; + 3.9 %] for column CO retrievals. The better observed performance is mainly due to the advantage of the finer model spatial resolution. WRF-Chem simulation showed low to moderate biases for major meteorological variables, except for sensible heat where a large bias (16-19 $W.m^{-2}$) is observed during the warm period. Furthermore, the results indicate some limitations in parameterization, such as the cumulus Tiedtke scheme leading to precipitation overestimation over widely-varying climate and topography regions e.g. high-elevation Tibetan plateau, Indo-Gangetic Plain region and Southeastern Asia.

The WRF-Chem reproduced well the overall spatial and seasonal variability of O_3, CO and AOD over the Asian region, but large discrepancies were found for NO_2 during the warm period. The observed bias between model-simulated and satellite-retrieved values were mainly attributed to uncertainties in satellite retrievals, vertical and horizontal model resolution, bottom-up emissions, anthropogenic and natural NO_x emission estimates (e.g. by lightning and soil), dust and $PM_{2.5}$ emission, stratosphere-to-troposphere O_3 exchange, transboundary pollution, low NO titration and uncertainty in N_2O_5 and nitrate radical reactions in the WRF-Chem chemical mechanism (Yegorova et al., 2011; Li et al., 2014; Parrish et al., 2014; Huang et al., 2017; Sicard et al., 2017; Zhang et al., 2016a; Mu et al., 2017).

For any application of models results, including reliable air pollution risk assessment, the generation of realistic maps is needed, particularly over highly complex terrain of Northern India (Indo-Gangetic Plain) where air quality is poor (Kumar et al., 2012a). Regional chemistry-climate models at coarse horizontal resolution are often unable to resolve the local features influencing the chemical transformation (Tie at al., 2010; Huang et al., 2017) and barely able to fully reproduce the ground observations (Schaap et al., 2015; Jonson et al., 2018) in particular at high-elevation sites (Strode et al., 2015). To date, the most damaging air pollutant for vegetation and human health are O_3 and PM (Sicard et al., 2016a, 2019). In this study, WRF-Chem model reproduced well the spatial and seasonal variability of surface NO_2, O_3, $PM_{2.5}$ and PM_{10} mean concentrations across China, following the recommended benchmarks for the chemical model performance for O_3 and NO_2. However, our results suggest that it is essential to improve the emission estimates of primary PM (e.g. new dust emission scheme) and NO_x (e.g. adjusted anthropogenic emission and vertical distribution) and upgrade chemical mechanisms e.g. Polycyclic Aromatic Hydrocarbon heterogeneous reactions with O_3 and homogeneous reaction with the nitrate radical in order to reduce bias in simulating the surface O_3 and PM concentrations over Asia (Zhang et al., 2016b; Mu et al., 2017).

Acknowledgments: We thank Dr Gabriele Pfister from the National Center for Atmospheric Research, Atmospheric Chemistry Observations and Modeling (Boulder, USA) for the provided recommendations, and technical support for data analysis. The computing resources

and the related technical support used for this work have been provided by CRESCO/ENEA-GRID High Performance Computing infrastructure and its staff (http://www.cresco.enea.it). CRESCO/ENEAGRID High Performance Computing infrastructure is funded by ENEA, the Italian National Agency for New Technologies, Energy and Sustainable Economic Development and by National and European research programs". Financial support from the LIFE15 ENV/IT/000183 project MOTTLES of the European Union, Chinese Academy of Sciences President's International Fellowship Initiative (PIFI) for Senior Scientists (Grant Number 2016VBA057). This work was carried out within the IUFRO Research Group 8.04.00 "Air Pollution and Climate Change".

Author contribution. P.S., A.A. and A.D.M. conceived the project. A.A., P.C., S.C., P.G. and J.C. carried out modelling. A.A., P.S., Z.Z., E.P. and A.D.M. analyzed the modelling outputs. All authors participated in writing of the manuscript, in particular P.S. and A.A.

Data availability. All data and figures are available in this paper. No more data are available.

Competing interests. The authors declare that they have no conflict of interest.

References

Amnuaylojaroen T., Macatangay R.C., Khodmanee S., 2019, "Modeling the effect of VOCs from biomass burning emissions on ozone pollution in upper Southeast Asia". Heliyon, 5: e02661.

Amnuaylojaroen T., Barth M.C., Emmons L.K., Carmichael G.R., Kreasuwun J., Prasitwattanaseree S., Chantara S., 2014, "Effect of different emission inventories on modeled ozone and carbon monoxide in Southeast Asia". Atmos. Chem. Phys., 14: 12,983-13.

Apte J.S., Brauer M., Cohen A.J., Ezzati M., Pope C.A., 2018, "Ambient $PM_{2.5}$ Reduces Global and Regional Life Expectancy". Environ. Sci. Technol. Lett., 5: 546-551.

Archer-Nicholls S., Lowe D., Utembe S., Allan J., Zaveri R.A., Fast J.D., Hodnebrog Ø., Denier van der Gon H., McFiggan G., 2014, "Gaseous chemistry and aerosol mechanism developments for version 3.5.1 of the online regional model, WRF-Chem". Geosci. Model Dev., 7: 2557–2579.

Barten J.G.M., Ganzeveld L.N., Visser A.J., Jiménez R., Krol M.C., 2019, "Evaluation of nitrogen oxides sources and sinks and ozone production in Colombia and surrounding areas". Atmos. Chem. Phys. Discuss. https://doi.org/10.5194/acp-2019-781.

Beelen R., Hoek G., Pebesma E., Vienneau D., de Hoogh K., Briggs D.J., 2009, "Mapping of background air pollution at fine spatial scale across the European Union". Sci. Total Environ., 407: 1852-1867.

Beirle S., Platt U., Wenig M., Wagner T., 2003, "Weekly cycle of NO_2 by GOME measurements: a signature of anthropogenic sources". Atmos. Chem. Phys., 3: 2225-2232.

Boden T.A., Andres R.J., Marland G., 2017, "Global, Regional, and National Fossil-Fuel CO_2 Emissions". Carbon Dioxide Information Analysis Center, Oak Ridge National Laboratory, U.S. Department of Energy, Oak Ridge, Tenn., U.S.A. doi 10.3334/CDIAC/00001_V2017.

Boersma K.F., Eskes H.J., Dirksen R.J., van der A R.J., Veefkind J. P., Stammes P., Huijnen V., Kleipool Q.L., et al., 2011, "An improved retrieval of tropospheric NO_2 columns from the Ozone Monitoring Instrument". Atmos. Meas. Tech., 4: 1905-1928.

Boylan J.W. and Russell A.G., 2006, "PM and light extinction model performance metrics, goals, and criteria for three dimensional air quality models". Atmos. Environ., 40: 4946-4959.

Burnett R., Chen H., Szyszkowicz M., Fann N., Hubbell B., Pope C.A., Apte J.S., Brauer M., et al., 2018, "Global estimates of mortality associated with long-term exposure to outdoor fine particulate matter". Proc. Natl. Acad. Sci. USA, 115: 9592-9597.

Chen S., Hamdi R., Uchenna Ochege F., Du H., Chen X., Yang W., Zhang C., 2019, "Added Value of a Dynamical Downscaling Approach for Simulating Precipitation and Temperature Over Tianshan Mountains Area, Central Asia". J. Geophys. Res.-Atmos., 124: 11051-11069.

Chen X.L., Ma Y.M., Kelder H., Su Z., Yang K., 2011, "On the behaviour of the tropopause folding events over the Tibetan Plateau". Atmos. Chem. Phys., 11: 5113-5122.

Chen F., and Dudhia J., 2001, "Coupling an advanced land surfacehydrology model with the Penn State–NCAR MM5 modeling system, Part I: Model implementation and sensitivity".Mon. Weather Rev., 129: 569-585.

Chin M., Rood R.B., Lin S.J., 2000, "Atmospheric sulfur cycle simulated in the global model GOCART: Model description and global properties". J. Geophys. Res., 105: 24671-24687.

Chuang M.T., Zhang Y., Kang D., 2011, "Application of WRF/Chem-MADRID for real-time air quality forecasting over the Southeastern United States". Atmos. Environ., 45: 6241-6250.

Cohen A.J, Brauer M., Burnett R., Anderson H.R., Frostad J., Estep K., Balakrishnan K., Brunekreef B., et al., 2017, "Estimates and 25–year trends of the global burden of disease attributable to ambient air pollution: an analysis of data from the Global Burden of Diseases Study 2015". Lancet, 389: 1907-1918.

Cooper O.R., Parrish D.D., Ziemke J., Balashov N.V., Cupeiro M., Galbally I.E., Gilge S., Horowitz L., et al., 2014, "Global distribution and trends of tropospheric ozone: An observation-based review". Elementa: Sci. Anthrop., 2: 000029.

Crippa P., Sullivan R.C., Thota A., Pryor S.C., 2019, "Sensitivity of simulated aerosol properties over eastern North America to WRF□Chem parameterizations". J. Geophys. Res.-Atmos., 124: 3365-3383.

Crippa P., Sullivan R.C., Thota A., Pryor S.C., 2017, "The impact of resolution on meteorological, chemical and aerosol properties in regional simulations with WRF-Chem". Atmos. Chem. Phys., 17: 1511-1528.

Crippa P., Sullivan R.C., Thota A., Pryor S.C., 2016, "Evaluating the skill of high-resolution WRF-Chem simulations in describing drivers of aerosol direct climate forcing on the regional scale". Atmos. Chem. Phys., 16: 397-416.

Cuesta J., Kanaya Y., Takigawa M., Dufour G., Eremenko M., Foret G., Miyazaki K., Beekmann M., 2018, "Transboundary ozone pollution across East Asia: daily evolution and photochemical production analysed by IASI + GOME2 multispectral satellite observations and models". Atmos. Chem. Phys., 18: 9499-9525.

Cuesta J., Eremenko M., Liu X., Dufour G., Cai Z., Höpfner M., von Clarmann T., Sellitto P., et al., 2013, "Satellite observation of lowermost tropospheric ozone by multispectral synergism of IASI thermal infrared and GOME-2 ultraviolet measurements over Europe". Atmos. Chem. Phys., 13: 9675-9693.

Deeter M.N., Emmons L.K., Francis G.L., Edwards D.P., Gille J.C., Warner J.X., Khattatov B., Ziskin D., et al., 2003, "Operational carbon monoxide retrieval algorithm and selected results for the MOPITT instrument". J. Geophys. Res., 108: 4399.

Emery C., Liu Z., Russell A.G., Talat Odman M., Yarwood G., Kumar N., 2017, "Recommendations on statistics and benchmarks to assess photochemical model performance".
J. Air Waste Manage. Assoc., 67: 582-598.

Emmons L.K., Walters S., Hess P.G., Lamarque J.-F., Pfister G.G., Fillmore D., Granier C., Guenther A., et al., 2010, "Description and evaluation of the Model for Ozone and Related chemical Tracers, version 4 (MOZART-4)". Geosci. Model Dev., 3: 43-67.

Feng Z., De Marco A., Anav A., Gualtieri M., Sicard P., Tian H., Fornasier F., Tao F., Guo A., Elena Paoletti, 2019, "Economic losses due to ozone impacts on human health, forest productivity and crop yield across China". Environ. Int. 131: 104966.

Feng Z., Hu E., Wang X., Jiang L., Liu X., 2015, "Ground-level O3 pollution and its impacts on food crops in China: A review". Environ. Pollut., 199: 42-48.

Fiore A.M., Dentener F.J., Wild O., Cuvelier C., Schultz M.G., Hess P., Textor C., Schulz M., et al., 2009, "Multimodel estimates of intercontinental source-receptor relationships for ozone pollution". J. Geophys. Res., 114, D04301.

Gao Y., Zhao C., Liu X., Zhang M., Leung L., 2014, "WRF-Chem simulations of aerosols and anthropogenic aerosol radiative forcing in East Asia". Atmos. Environ., 92: 250-266.

Georgiou G.K., Christoudias T., Proestos Y., Kushta J., Hadjinicolaou P., Lelieveld J., 2018, "Air quality modelling in the summer over the eastern Mediterranean using WRF-Chem: chemistry and aerosol mechanism intercomparison". Atmos. Chem. Phys., 18: 1555-1571.

Ghim Y.S., Choi Y., Kim S., Bae C.H., Park J., Shin H.J., 2017, "Evaluation of Model Performance for Forecasting Fine Particle Concentrations in Korea". Aero Air Qual. Res., 17: 1856-1864.

Giani P., Anav A., De Marco A., Feng Z., Crippa P., 2020, "Exploring sources of uncertainty in premature mortality estimates from fine particulate matter: the case of China". Environ. Res. Lett. in press https://doi.org/10.1088/1748-9326/ab7f0f

Ginoux P., Chin M., Tegen I., Prospero J.M., Holben B., Dubovik O., Lin S.J., 2001, "Sources and distributions of dust aerosols simulated with the GOCART model". J. Geophys. Res.-Atmos., 106: 20,255-20,273.

Goldemberg J., Martinez-Gomez J., Sagar A., Smith K., 2018, "Household air pollution, health, and climate change-clearing the air". Environ. Res. Lett., 13: 030201.

Gong S.L., 2003, "A parameterization of sea-salt aerosol source function for sub- and super-micron particles". Global Biogeochem. Cy., 17: 1097.

Grell G.A., Peckham S.E., Schmitz R., McKeen S.A., Frost G., Skamarock W.C., Eder B., 2005, "Fully coupled "online" chemistry within the WRF model". Atmos. Environ., 39: 6957– 6975.

Guenther A.B., Jiang X., Heald C.L., Sakulyanontvittaya T., Duhl T., Emmons L.K., Wang X., 2012, "The Model of Emissions of Gases and Aerosols from Nature version 2.1 (MEGAN2.1): an extended and updated framework for modeling biogenic emissions". Geosci. Model Dev., 5: 1471-1492.

Hall D.K. and Riggs G.A., 2015, "MODIS/Aqua Sea Ice Extent 5-Min L2 Swath 1km. Version 6". Boulder, Colorado USA: NASA National Snow and Ice Data Center Distributed Active Archive Center. http://dx.doi.org/10.5067/MODIS/MYD29.006

Hall D.K., Riggs G.A., Foster J.L., Kumar S., 2010, "Development and validation of a cloud-gap filled MODIS daily snow-cover product". Remote Sensing of Environment, 114: 496-503.

Hong S.Y., and Lim J.O.J., 2006, "The WRF single–moment 6–class microphysics scheme (WSM6)". J. Korean Meteor. Soc., 42, 129-151.

Hong S.Y., Noh Y., Dudhia J., 2006, "A new vertical diffusion package with an explicit treatment of entrainment processes". Mon. Weather Rev., 134: 2318-2341.

Huang M., Carmichael G.R., Pierce R.B., Jo D.S., Park R.J., Flemming J., Emmons L.K., Bowman K.W., et al., 2017, "Impact of intercontinental pollution transport on North American ozone air pollution: An HTAP phase 2 multi-model study". Atmos. Chem. Phys., 17: 5721-5750.

Huijnen V., Wooster M.J., Kaiser J.W., Gaveau D.L.A., Flemming J., Parrington M., Inness A., Murdiyarso D., Main B., van Weele M., 2016, "Fire carbon emissions over maritime southeast Asia in 2015 largest since 1997". Scientific Reports, 6: 26886.

Iacono M.J., Delamere J.S., Mlawer E.J., Shephard M.W., Clough S.A., Collins W.D., 2008, "Radiative forcing by long–lived greenhouse gases: Calculations with the AER radiative transfer models". J. Geophys. Res., 113: D13103.

Im U., Bianconi R., Solazzo E., Kioutsioukis I., Badia A., Balzarini A., Baro R., Bellasio R., et al., 2015. "Evaluation of operational online-coupled regional air quality models over Europe and North America in the context of AQMEII phase 2. Part I: ozone". Atmos. Environ., 115: 404-420.

Janssens-Maenhout G., Crippa M., Guizzardi D., Dentener F., Muntean M., Pouliot G., Keating T., Zhang Q., et al., 2015, "HTAP_v2.2: a mosaic of regional and global emission grid maps for 2008 and 2010 to study hemispheric transport of air pollution". Atmos. Chem. Phys., 15: 11411-11432.

Jena C., Ghude S.D., Beig G., Chate D.M., Kumar R., Pfister G.G., Lal D.M., Surendran D.E., et al., 2015, "Inter-comparison of different NOx emission inventories and associated variation in simulated surface ozone in Indian region". Atmos. Environ., 117: 61-73.

Jonson J.E., Schulz M., Emmons L., Flemming J., Henze D., Sudo K., Tronstad Lund M., Lin M., et al., 2018, "The effects of intercontinental emission sources on European air pollution levels". Atmos. Chem. Phys., 18: 13655-13672.

Juneng L., Tangang F., Chung J.X., Ngai S.T., The T.W., Narisma G., Cruz F., Phan-Van T., et al., 2016, "Sensitivity of the Southeast Asia Rainfall Simulations to Cumulus and Ocean Flux Parameterization in RegCM4". Clim. Res., 69: 59-77.

Jung M., Reichstein M., Bondeau A., 2009, "Towards global empirical upscaling of FLUXNET eddy covariance observations: Validation of a model tree ensemble approach using a biosphere model". Biogeosciences, 6: 2001-2013.

Jung M., Reichstein M., Margolis H.A., Cescatti A., Richardson A.D., Arain M.A., Arneth A., Bernhofer C., et al., 2011, "Global patterns of land-atmosphere fluxes of carbon dioxide, latent heat, and sensible heat derived from eddy covariance, satellite, and meteorological observations". J. Geophys. Res.- Biogeo., 116: G00J07.

Karlický J., Huszár P., Halenk T., 2017, "Validation of gas phase chemistry in the WRF-Chem model over Europe". Adv. Sci. Res., 14: 181-186.

Krishna B., Balakrishnan K., Siddiqui A.R., Begum B.A., Bachani D., Brauer M., 2017, "Tackling the health burden of air pollution in South Asia". BMJ 359, BMJ, 359: j5209.

Kumar R., Barth M.C., Nair V.S., Pfister G.G., Suresh Babu S., Satheesh S.K., Krishna Moorthy K., Carmichael G.R., et al., 2015, "Sources of black carbon aerosols in South Asia and surroundingregions during the Integrated Campaign for Aerosols, Gases and Radiation Budget (ICARB)". Atmos. Chem. Phys., 15: 5415-5428.

Kumar R., Naja M., Pfister G.G., Barth M.C., Wiedinmyer C., Brasseur G.P., 2012a, "Simulations over South Asia using the weather research and forecasting model with chemistry (WRF-Chem): chemistry evaluation and initial results". Geosci. Model Dev. Discuss., 5: 1-66.

Kumar R., Naja M., Pfister G.G., Barth M.C., Brasseur G.P., 2012b, "Simulations over South Asia using the Weather Research and Forecasting model with Chemistry (WRF-Chem): set-up and meteorological evaluation". Geosci. Model Dev., 5: 321-343.

Landrigan P.J., Fuller R., Acosta N.J.R., Adeyi O., Arnold R., Basu N., Baldé A.B., Bertollini R., et al., 2017, "The Lancet Commission on pollution and health". Lancet 6736.

Lefohn A.S., Malley C.S., Simon H., Wells B., Xu X., et al., 2017, "Responses of human health and vegetation exposure metrics to changes in ozone concentration distributions in the European Union, United States, and China". Atmos. Environ., 152: 123-145.

Lelieveld J., Evans J.S., Fnais M., Giannadaki D., Pozzer A., 2015, "The contribution of outdoor air pollution sources to premature mortality on a global scale". Nature, 525: 367-371.

Li P., Feng Z., Catalayud V., Yuan X., Xu Y., Paoletti E., 2017, "A meta-analysis on growth, physiological, and biochemical responses of woody species to ground-level ozone highlights the role of plant functional types". Plant Cell Environ., 40: 2369-2380.

Li X., Liu J., Mauzerall D.L., Emmons L.K., Walters S., Horowitz L.W., Tao S., 2014, "Effects of trans-Eurasian transport of air pollutants on surface ozone concentrations over Western China". J. Geophys. Res.-Atmos., 119: 12,338-12,354.

Li N., Lu Y., Liao H., He Q., Li J., Long X., 2018, "WRF-Chem modeling of particulate matter in the Yangtze River Delta region: Source apportionment and its sensitivity to emission changes". PLoS ONE, 13: e0208944.

Lin C., Chen D., Yang K., Ou T., 2018, "Impact of model resolution on simulating the water vapor transport through the central Himalayas: implication for models' wet bias over the Tibetan Plateau". Climate Dynamics 51: 3195-3207.

Liu M., Lin J., Wang Y., Sun Y., Zheng B., Shao J., Chen L., Zheng Y., et al., 2018, "Spatiotemporal variability of NO_2 and $PM_{2.5}$ over Eastern China: observational and model analyses with a novel statistical method". Atmos. Chem. Phys., 18: 12933-12952.

Liu J., Han Y., Tang X., Zhu J., Zhu T., 2016, "Estimating adult mortality attributable to $PM_{2.5}$ exposure in China with assimilated $PM_{2.5}$ concentrations based on a ground monitoring network". Sci. Total Environ., 568: 1253-1262.

Liu Z., Guan D., Wei W., Davis S.J., Ciais P., Bai J., Peng S., Zhang Q., et al., 2015, "Reduced carbon emission estimates from fossil fuel combustion and cement production in China". Nature, 524: 335-338.

Ma J. and van Aardenne J.A., 2004, "Impact of different emission inventories on simulated tropospheric ozone over China: a regional chemical transport model evaluation". Atmos. Chem. Phys., 4: 877-887.

Ma N., Niu G□Y., Xia Y., Cai X., Zhang Y., Ma Y., Fang Y., 2017, "A Systematic Evaluation of Noah-MP in Simulating Land-Atmosphere Energy, Water, and Carbon Exchanges Over the Continental United States". J. Geophys. Res.-Atmos., 122: 12,245-12,268.

Malardel S., Wedi N., Deconinck W., Diamantakis M., Kühnlein C., Mozdzynski G., et al., 2016, "A new grid for the IFS. ECMWF Newsletter 146: 23-28.

Mar K.A, Ojha N., Pozzer A., Butler, T.M., 2016. "Ozone air quality simulations with WRF-Chem (v3.5.1) over Europe: model evaluation and chemical mechanism comparison". Geosci. Model Dev., 9: 3699-3728.

McKeen S., Wilczak J., Grell G., Djalalova I., Peckham S., Hsie E.Y., Gong W., Bouchet V., et al., 2005, "Assessment of an ensemble of seven real-time ozone forecasts over eastern North America during the summer of 2004". J. Geophys. Res. - Atmos., 110: D21307.

Mead M.I., Castruccio S., Latif M.T., Nadzir M.S.M., Dominick D., Thota A., Crippa P., 2018, "Impact of the 2015 wildfires on Malaysian air quality and exposure: a comparative study of observed and modeled data". Environ. Res. Lett., 13: 4.

MEP - Ministry of Environmental Protection, 2012, "Government of China, Ambient Air Quality Standards (in Chinese)". GB 3095-2012.

Mitchell T.D. and Jones P.D., 2005, "An improved method of constructing a database of monthly climate observations and associated high-resolution grids". Int. J. Climatol., 25: 693-712.

Monks P.S., Archibald A.T., Colette A., Cooper O., Coyle M., Derwent R., Fowler D., Granier C., et al., 2015, "Tropospheric ozone and its precursors from the urban to the global scale fromair quality to short-lived climate forcer". Atmos. Chem. Phys., 15: 8889-8973.

Mooney P.A., Mulligan F.J., Fealy R., 2013, "Evaluation of the Sensitivity of the Weather Research and Forecasting Model to Parameterization Schemes for Regional Climates of Europe over the Period 1990-95". American Meteorological Society. Journal of climate 26: 1002-1017.

Morris R.E., McNally D.E., Tesche T.W., Tonnesen G., Boylan J.W., Brewer P., 2005, "Preliminary Evaluation of the Community Multiscale Air Quality Model for 2002 over the Southeastern United States. J. Air Waste Manag. Assoc., 55: 1694-1708.

Mu Q., Lammel G., Gencarelli C.N., Hedgecock I.M., Chen Y., Přibylová P., Teich M., Zhang Y., et al., 2017, "Regional modelling of polycyclic aromatic hydrocarbons: WRF-Chem-PAH model development and East Asia case studies". Atmos. Chem. Phys., 17: 12,253-12,267.

Parrish D.D., Lamarque J.F., Naik V., Horowitz L., Shindell D.T., Staehelin J., Derwent R., Cooper O.R., et al., 2014, "Long-term changes in lower tropospheric baseline ozone concentrations: Comparing chemistry-climate models and observations at northern mid-latitudes". J. Geophys. Res.-Atmos., 119: 5719-5736.

Pope R.J., Savage N.H., Chipperfield M.P., Arnold S.R., Osborn T.J., 2015, "The influence of synoptic weather regimes on UK air quality: analysis of satellite column NO_2". Atmospheric Science Letters 15: 211-217.

Prodhomme C., Batté L., Massonnet F., Davini P., Bellprat O., Guemas V., et al., 2016, "Benefits of Increasing the Model Resolution for the Seasonal Forecast Quality in EC-Earth". J. Climate 29: 9141-9162.

Quéré C.L.E., Moriarty R., Andrew R.M., Canadell J.G., Sitch S., Korsbakken J.I., Friedlingstein P., Peters G.P., et al., 2015, "Global Carbon Budget 2015". Earth Syst. Sci. Data, **7**: 349-396.

Randall D.A., Wood R.A., et al., 2007, "Climate models and their evaluation. Climate Change

2007: The Physical Science Basis". S. Solomon et al., Eds., Cambridge University Press, 589-662.

Ratna S.B., Ratnam J.V., Behera S.K., Rautenbach C.J., Ndarana T., Takahashi K., Yamagata T., 2014, "Performance assessment of three convective parameterization schemes in WRF for downscaling summer rainfall over South Africa". Clim Dyn, 42: 2931-2953.

Reddington C.L., Conibear L., Knote C., Silver B.J., Li Y.J., Chan C.K., Arnold S.R., Spracklen D.V., 2019, "Exploring the impacts of anthropogenic emission sectors on $PM_{2.5}$ and human health in South and East Asia". Atmos. Chem. Phys., 19: 11,887-11,910.

Ritter M., M.D., Müller, Tsai M.Y., Parlow E., 2013, "Air pollution modeling over very complex terrain: An evaluation of WRF-Chem over Switzerland for two 1-year periods". Atmos. Res., 132-133: 209-222.

Roebber P.J., Schultz D.M., Colle B.A., Stensrud D.J., 2004, "Toward Improved Prediction: High-Resolution and Ensemble Modeling Systems in Operations". Wea. Forecasting 19: 936-949.

Roy S., Beig G., Jacob D., 2008, "Seasonal distribution of ozone and its precursors over the tropical Indian region using regional chemistry-transport model". J. Geophys. Res., 113: D21307.

Ryu Y.H., Hodzic A., Barre J., Descombes G., Minnis P., 2018, "Quantifying errors in surface ozone predictions associated with clouds over the CONUS: a WRF-Chem modeling study using satellite cloud retrievals". Atmos. Chem. Phys., 18: 7509-7525.

Sagar A.D., Balakrishnan K., Guttikunda S.K., Roychowdhury A., 2016, "India Leads the Way: A Health-Centered Strategy for Air Pollution". Environ. Health Perspect., 124: A116–A117.

Savage N.H., Agnew P., Davis L.S., Ordóñez C., Thorpe R., Johnson C.E., O'Connor F.M., Dalvi M., 2013, "Air quality modelling using the Met Office Unified Model (AQUM OS24-26): model description and initial evaluation". Geosci. Model Dev., 6: 353-372.

Schaap M., Cuvelier C., Hendriks C., Bessagnet B., Baldasano J., Colette A., Thunis P., Karam D., et al., 2015, "Performance of European chemistry transport models as function of horizontal resolution". Atmos. Environ., 112: 90-105.

Schürmann G.J., Algieri A., Hedgecock I.M., Manna G., Pirrone N., Sprovieri F., 2009, "Modelling local and synoptic scale influences of ozone concentrations in a topographically complex region of Southern Italy". Atmos. Environ., 43: 4424–4434.

Sharma A., Ojha N., Pozzer A., Mar K.A., Beig G., Lelieveld J., Gunthe S.S., 2017, "WRF-Chem simulated surface ozone over south Asia during the re-monsoon: effects of emission inventories and chemical mechanisms". Atmos. Chem. Phys., 17: 14393-14413.

Shindell D.T., Lamarque J.F., Schulz M., Flanner M., Jiao C., Chin M., Young J., Lee Y.H., et al., 2013, "Radiative forcing in the ACCMIP historical and future climate simulations". Atmos. Chem. Phys., 13: 2939-2974.

Sicard P., Khaniabadi Y.O., Perez S., Gualtieri M., De Marco A., 2019, "Effect of O_3, PM_{10} and $PM_{2.5}$ on cardiovascular and respiratory diseases in cities of France, Iran and Italy". Environ. Sci. Pollut. Res. 1-21.

Sicard P., Anav A., De Marco A., Paoletti E., 2017, "Projected global tropospheric ozone impacts on vegetation under different emission and climate scenarios". Atmos. Chem. Phys., 17: 12177–12196.

Sicard P., Augustaitis A., Belyazid S., Calfapietra C., De Marco A., Fenn M., Grulke N., He S., et al., 2016a, "Global topics and novel approaches in the study of air pollution, climate change and forest ecosystems". Environ. Pollut., 213: 977-987.

Sicard P., Serra R., Rossello P., 2016b, "Spatio-temporal trends of surface ozone concentrations and metrics in France." Environ. Res., 149: 122-144.

Sicard P., Coddeville P., Galloo J.C., 2009, "Near-surface ozone levels and trends at rural stations in France over the 1995-2003 period". Environ. Monit. Assess., 156: 141-157.

Skamarock W.C. and Klemp J.B., 2008, "A time-split non-hydrostatic atmospheric model for weather research and forecasting applications". J. Comput. Phys., 227: 3465-3485.

Solazzo E., Bianconi R., Vautard R., Appel K.W., Moran M.D., Hogrefe C., Bessagnet B., Brandt J., et al., 2012, "Model evaluation and ensemble modelling of surface-level ozone in Europe and North America in the context of AQMEII". Atmos. Environ., 53: 60-74.

Spiridonov V., Jakimovski B., Spiridonova I., Pereira G., 2019, "Development of air quality forecasting system in Macedonia, based on WRF-Chem model". Air Qual. Atmos. Health, 12: 825-836.

Streets D.G., Bond T.C., Carmichael G.R., Fernandes S.D., Fu Q., He D., Klimont Z., Nelson S.M., et al., 2003, "An inventory of gaseous and primary aerosol emissions in Asia in the year 2000". J. Geophys. Res., 108: 8809.

Strode S.A., Rodriguez J.M., Logan J.A., Cooper O.R., Witte J.C., Lamsal L.N., Damon M., Van Aartsen B., et al., 2015, "Trends and variability in surface ozone over the United States". J. Geophys. Res.-Atmos., 120: 9020–9042.

Tai A.P., Martin M.V., Heald C.L., 2014, "Threat to future global food security from climate change and ozone air pollution". Nat. Clim. Change, 4: 817-821.

Tang J., Wang S., Niu X., Hui P., Zong P., Wang X., 2017, "Impact of spectral nudging on regional climate simulation over CORDEX East Asia using WRF". Clim. Dyn., 48: 2339-2357.

Tang H., Takigawa M., Liu G., Zhu J., Kobayashi K., 2013, "A projection of ozone-induced wheat production loss in China and India for the years 2000 and 2020 with exposure-based and flux-based approaches". Glob. Change Biol., 19: 2739-2752.

Tao Z., Larson S.M., Williams A., Caugheyc M., Wuebbles D.J., 2004, "Sensitivity of regional ozone concentrations to temporal distribution of emissions". Atmos. Environ., 38: 6279-6285.

Tian H. Ren W., Tao B., Sun G., Chappelka A., Wang X., Pan S., Yang J., et al., 2016, "Climate extremes and ozone pollution: a growing threat to China's food security". Ecosystem Health and Sustainability, 2: e01203.

Tie X., Brasseur G., Ying Z., 2010, "Impact of model resolution on chemical ozone formation in Mexico City: application of the WRF-Chem model". Atmos. Chem. Phys., 10: 8983-8995.

Tie X., Madronich S., Li G., Ying Z., Zhang R., Garcia A., Lee-Taylor J., Liu Y., 2007, "Characterization of chemical oxidants in Mexico City: A regional chemical dynamical model (WRF-CHEM) study". Atmos. Environ., 41: 1989-2008.

Tuccella P., Curci G., Visconti G., Bessagnet B., Menut L., Park R.J., 2012, "Modeling of gas and aerosol with WRF-Chem over Europe: Evaluation and sensitivity study". J. Geophys. Res. - Atmos., 117: D03303.

Vannière B., Demory M.E., Vidale P.L., Schiemann R., Roberts M.J., Roberts C.D., et al., 2019, "Multi-model evaluation of the sensitivity of the global energy budget and hydrological cycle to resolution". Climate Dynamics 52: 6817-6846.

Venkataraman C., Brauer M., Tibrewal K., Sadavarte P., Ma Q., Cohen A., Chaliyakunnel S., Frostad J., et al., 2018, "Source influence on emission pathways and ambient $PM_{2.5}$ pollution over India (2015-2050)". Atmos. Chem. Phys., 18: 8017-8039.

Visser A.J., Folkert Boersma K., Ganzeveld L.N., Krol M.C., 2019, "European NOx emissions in WRF-Chem derived from OMI: impacts on summertime surface ozone". Atmos. Chem. Phys., 19: 11821-11841.

Wang L., Zhang F., Pilot E., Yu J., Nie C., Holdaway J., Yang L., Li Y., et al., 2018, "Taking Action on Air Pollution Control in the Beijing-Tianjin-Hebei (BTH) Region: Progress, Challenges and Opportunities". Int. J. Environ. Res. Public Health, 15: 306.

Wang W.N., Cheng T.H., Gu X.F., Chen H., Guo H., Wang Y., Bao F.W., Shi S.Y., et al., 2017a, "Assessing Spatial and Temporal Patterns of Observed Ground-level Ozone in China". Scientific Reports, 7: 3651.

Wang Z., Duan A., Yang S., Ullah K., 2017b, "Atmospheric moisture budget and its regulation on the variability of summer precipitation over the Tibetan Plateau". J. Geophys. Res., 122: 614-630.

Wang Z., Duan A., Li M., He B., 2016, "Influences of thermal forcing over the slope/platform of the Tibetan Plateau on Asian summer monsoon: numerical studies with WRF model". Chin. J. Geophys., 59: 474-487.

Wang Z., Duan A., Wu G., 2014, "Time-lagged impact of spring sensible heat over the Tibetan Plateau on the summer rainfall anomaly in East China: case studies using the WRF model". Clim. Dyn., 42: 2885-2898.

Wang X., Liang X.Z., Jiang W., Tao Z., Wang J.X.L., Liu H., Han Z., Liu S., et al., 2010, "WRF-Chem simulation of East Asian air quality: Sensitivity to temporal and vertical emissions distributions". Atmos. Environ., 44: 660-669.

Werner M., Kryza M., Skjøth C.A., Wałaszek K., Dore A.J., Ojrzyńska H., Kapłon J., 2017, "Aerosol-Radiation Feedback and PM10 Air Concentrations Over Poland". Pure Appl. Geophys. 174: 551-568.

Wiedinmyer C., Akagi S.K., Yokelson R.J., Emmons L.K., Al-Saadi J.A., Orlando J.J, Soja A.J., et al., 2011, "The Fire INventory from NCAR (FINN): a high-resolution global model to estimate the emissions from open burning". Geosc. Mod. Dev., 4: 625-641.

Wittig V.E. Ainsworth E.A., Naidu S.L., Karnosky D.F., Long S.P., 2009, "Quantifying the impact of current and future tropospheric ozone on tree biomass, growth, physiology and biochemistry: a quantitative meta-analysis". Glob. Change Biol., 15: 396-424.

Wu Z., Wang X., Chen F., Turnipseed A.A., Guenther A.B., Niyogi D., Charusombat U., Xia B., Munger J.W., Alapaty K., 2011, "Evaluating the calculated dry deposition velocities of reactive nitrogen oxides and ozone from two community models over a temperate deciduous forest". Atmos. Environ., 45: 2663-2674.

Xu R., Tie X., Li G., Zhao S., Cao J., Feng T., Long X., 2018, "Effect of biomass burning on black carbon (BC) in South Asia and Tibetan Plateau: The analysis of WRF-Chem modeling". Sci. Total Environ., 645: 901-912.

Yahya K., Wang K., Gudoshava M., Glotfelty T., Zhang Y., 2015, "Application of WRF/Chem over North America under the AQMEII Phase 2: Part I. Comprehensive evaluation of 2006 simulation". Atmos. Environ., 115: 733-755.

Yegorova E.A., Allen D.J., Loughner C.P., Pickering K.E., Dickerson R.R., 2011, "Characterization of an eastern U.S. severe air pollution episode using WRF/Chem." J. Geophys. Res. - Atmos., 116: 1-21.

Zhang L., Li Q., Wang T., Ahmadov R., Zhang Q., Li M., Lv M., 2017, "Combined impacts of nitrous acid and nitryl chloride on lower-tropospheric ozone: new module development in WRF-Chem and application to China". Atmos. Chem. Phys., 17: 9733-9750.

Zhang Y., Zhang X., Wang L., Zhang Q., Duan F., He K., 2016a, "Application of WRF/Chem over East Asia: Part I. Model evaluation and intercomparison with MM5/CMAQ". Atmos. Environ., 124: 285-300.

Zhang Y., Zhang X., Wang L., Zhang Q., Duan F., He K., 2016b, "Application of WRF/Chem over East Asia: Part II. Model improvement and sensitivity simulations". Atmos. Environ., 124: 301-320.

Zhang L., Wu P., Zhou T., Roberts M.J., Schiemann R., 2016c, "Added value of high-resolution models in simulating global precipitation characteristics". Atmospheric Sci. Lett. 17: 646-657.

Zhang Y.L. and Cao F., 2015, "Fine particulate matter ($PM_{2.5}$) in China at a city level". Scientific Reports, 5: 14884.

Zhang C., Wang Y., Hamilton K., 2011, “Improved representation of boundary layer clouds over the southeast pacific in ARW–WRF using a modified Tiedtke cumulus parameterization scheme”. Mon. Weather Rev., 139: 3489-3513.

Zhong M., Saikawa E., Y. Liu, V. Naik, Horowitz L.W., Takigawa M., Zhao Y., Lin N-H., Stone E.A., 2016, “Air quality modeling with WRF-Chem v3.5 in East Asia: sensitivity to emissions and evaluation of simulated air quality”. Geosci. Model Dev., 9: 1201-1218.

1210 **Table 1.** Model set up with main physical and chemical schemes adopted in the simulation.

Model set-up	**Values**
Domain	South-East Asia
Simulation period	1st January - 31st December 2015
Spin up	20st December - 31st December 2014
Horizontal resolution	8 km
Vertical resolution	30 eta levels up to 50 hPa
Domain size	780 x 690 cells (lon x lat)
Meteorological boundary	ERA5 (31 km), 3h
Chemical boundary	**MOZART-4/GEOS-5**
Physical option	**Adopted scheme**
Microphysics	Single–moment 6–class
Cumulus Parameterization	New Tiedtke
Shortwave Radiation	RRTMG
Longwave Radiation	RRTMG
Land-surface	Noah Land Surface Model
Planetary boundary layer	Yonsei University Scheme
Chemical options	**Adopted scheme**
Gas phase chemistry	MOZART
Aerosols	GOCART
Photolysis	Madronich F-TUV
Biogenic emissions	MEGAN
Anthropogenic emissions	EDGAR HTAP (v2.2)
Fire emissions	FINN (v1.5)

1211

1212

1213

Table 2. Pearson's correlation coefficient (r) and mean bias (model-reference) computed using WRF results and different reference datasets for surface air temperature, precipitation, relative humidity, latent heat, sensible heat and snow cover fraction. Note that reference data were re-gridded to the WRF domain; in addition to downscale temperature we used a dry adiabatic lapse rate correction.

VARIABLE	REFERENCE	Pearson's correlation coefficient (r)				Mean bias			
		JFM	*AMJ*	*JAS*	*OND*	*JFM*	*AMJ*	*JAS*	*OND*
TEMPERATURE (°C)	ERA5	0.99	0.99	0.99	0.99	-1.51	-0.42	0.07	-0.68
	CRU	0.98	0.99	0.99	0.99	-1.82	-0.82	-0.20	-1.20
PRECIPITATION (mm/day)	ERA5	0.80	0.90	0.91	0.88	-0.04	0.15	0.27	-0.05
	CRU	0.73	0.84	0.84	0.81	0.25	0.74	0.68	0.21
RELATIVE HUMIDITY (%)	ERA5	0.99	0.99	0.99	0.99	-1.5	-3.1	-4.5	-4.0
	CRU	0.95	0.96	0.97	0.96	2.1	11.0	12.0	2.7
LATENT HEAT (W/m^2)	ERA5	0.92	0.94	0.95	0.94	2.0	0.5	2.6	-0.24
	MTE	0.95	0.97	0.97	0.95	3.0	6.3	13.2	4.6
SENSIBLE HEAT (W/m^2)	ERA5	0.88	0.94	0.93	0.87	-1.2	16.4	19.4	2.2
	MTE	0.82	0.93	0.91	0.87	-2.8	7.9	11.5	1.5
SNOW COVER FRACTION (%)	ERA5	0.95	0.84	0.74	0.89	-3.0	-3.2	-0.9	-2.7
	MODIS	0.92	0.89	0.77	0.92	0.6	0.2	-0.08	-1.7

JFM: January-February-March, AMJ: April-May-June, JAS: July-August-September, OND: October-November-December.

1223 **Table 3.** Pearson's correlation coefficient (r) and fractional bias computed using WRF-Chem
1224 results and different reference datasets for surface nitrogen dioxide (NO_2), aerosol optical
1225 depth (AOD), ozone (O_3) and carbon monoxide (CO) concentrations.

VARIABLE	REFERENCE	Pearson's correlation coefficient (r)				Fractional bias			
		JFM	*AMJ*	*JAS*	*OND*	*JFM*	*AMJ*	*JAS*	*OND*
NO_2	OMI	0.91	0.89	0.90	0.89	-2%	-64%	-70%	-8%
CO	MOPITT	0.97	0.97	0.96	0.97	-7%	7%	8%	3%
O_3	IASI	0.76	0.61	0.99	0.43	13%	3%	7%	11%
AOD	MODIS	0.93	0.88	0.86	0.91	-19%	6%	20%	-2%

1226 *JFM: January-February-March, AMJ: April-May-June, JAS: July-August-September, OND: October-*
1227 *November-December.*

1228

1229

1230 **Table 4.** Pearson's correlation coefficient, mean bias and fractional bias computed using
1231 WRF-Chem daily results at surface layer and ground measurements for surface nitrogen
1232 dioxide (NO_2), ozone (O_3), particulate matters ($PM_{2.5}$ and PM_{10}) concentrations; results
1233 represent the mean computed over all the available stations.

1234

VARIABLE	Pearson's correlation coefficient (r)	Mean bias	Fractional bias			
			JFM	*AMJ*	*JAS*	*OND*
NO_2	0.29	10.1 ppb	38%	35%	42%	45%
O_3	0.51	5.0 ppb	-8%	23%	24%	-14%
$PM_{2.5}$	0.44	10.4 µg m^{-3}	5%	20%	36%	23%
PM_{10}	0.35	14.8 µg m^{-3}	5%	11%	29%	24%

1235 *JFM: January-February-March, AMJ: April-May-June, JAS: July-August-September, OND:*
1236 *October-November-December.*

1237

1238

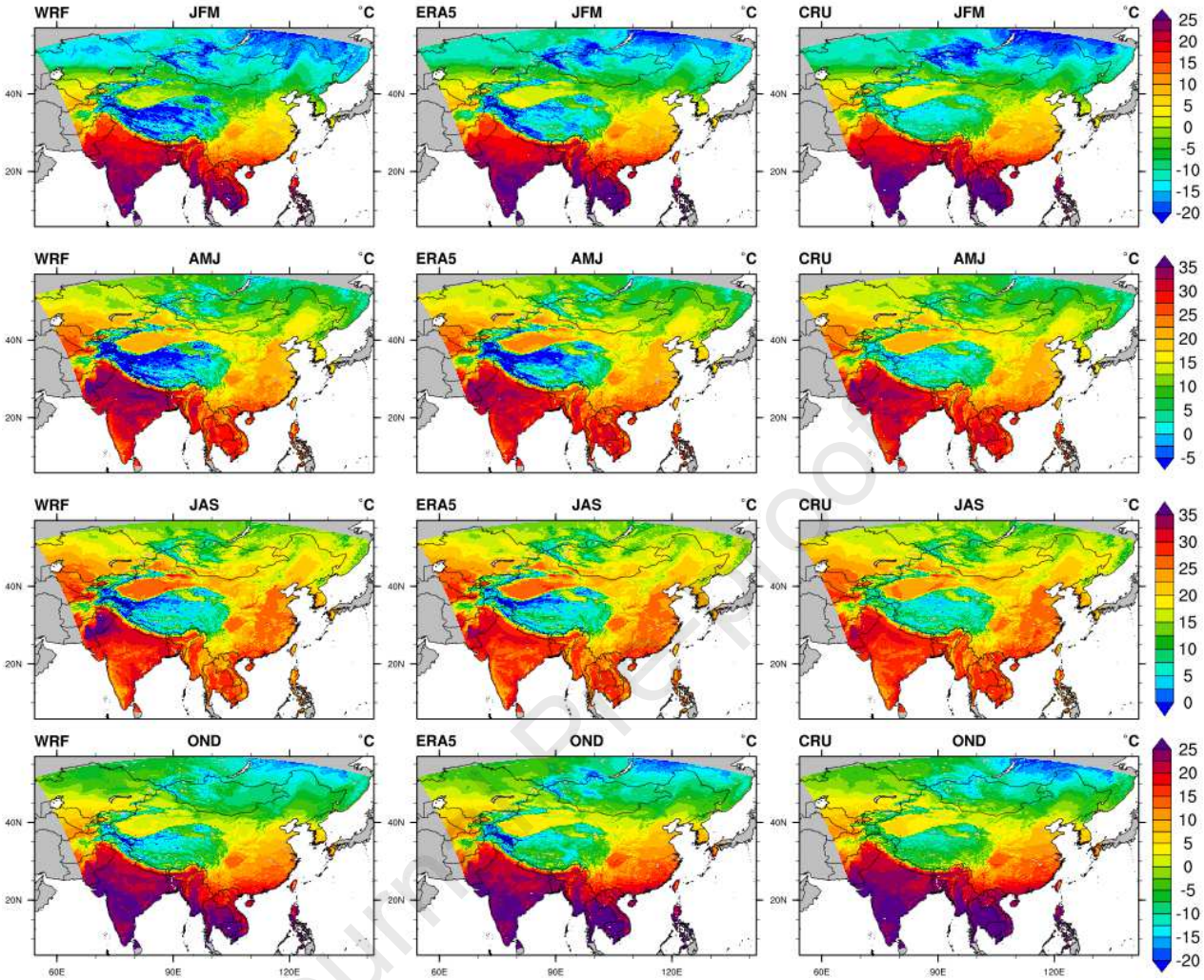

Figure 1. Spatial pattern of 2-meter air temperature (°C) as simulated by WRF-Chem (left panels) and compared to ERA5 reanalysis (central panels) and CRU dataset (right panels) during different seasons (JFM: January-February-March, AMJ: April-May-June, JAS: July-August-September, OND: October-November-December) in 2015. Mind the differences in color scales between seasonal climatologies.

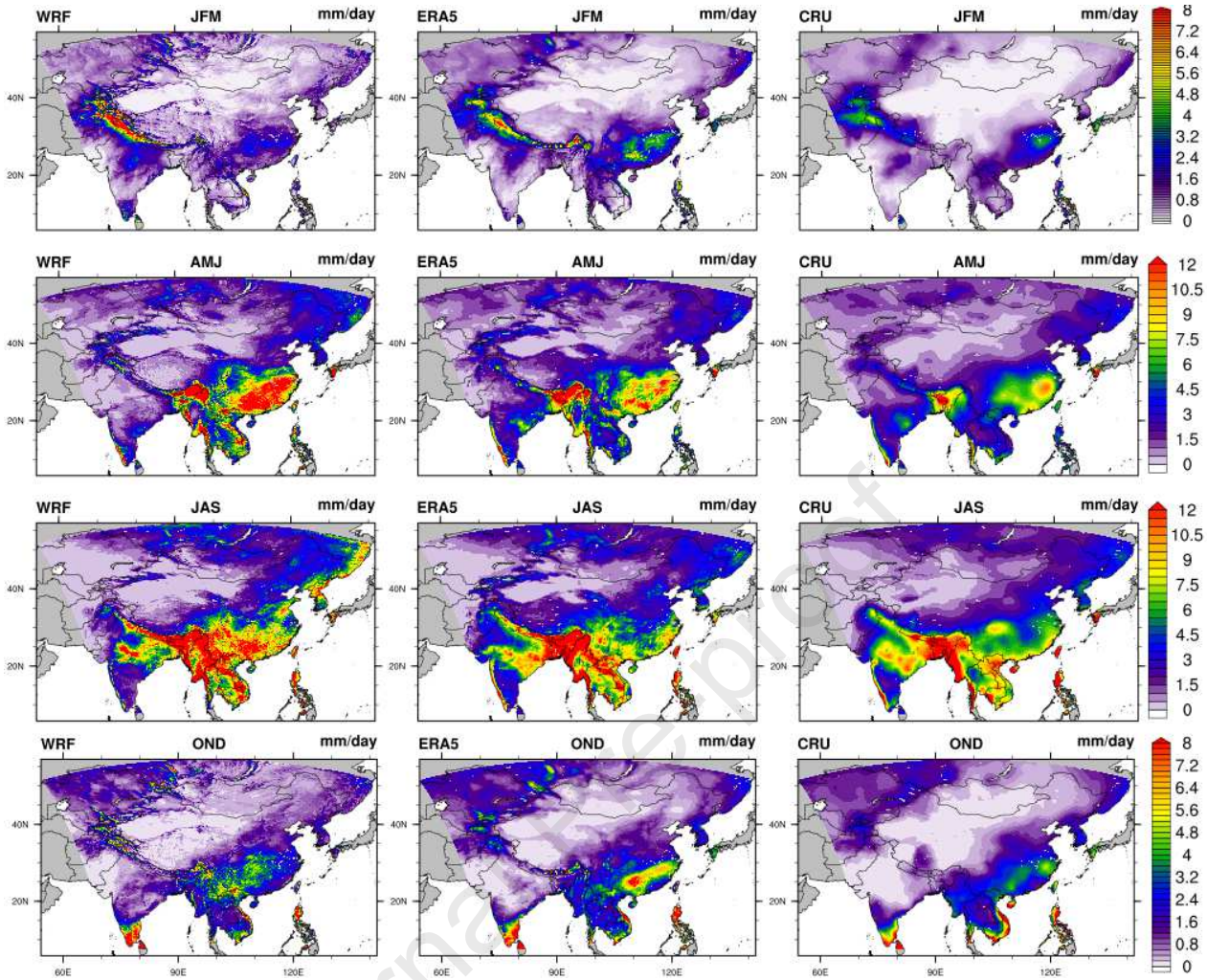

Figure 2. Spatial pattern of precipitation (mm/day) as simulated by WRF-Chem (left panels) and compared to ERA5 reanalysis (central panels) and CRU dataset (right panels) during different seasons (JFM: January-February-March, AMJ: April-May-June, JAS: July-August-September, OND: October-November-December). Mind the differences in color scales between seasonal climatologies.

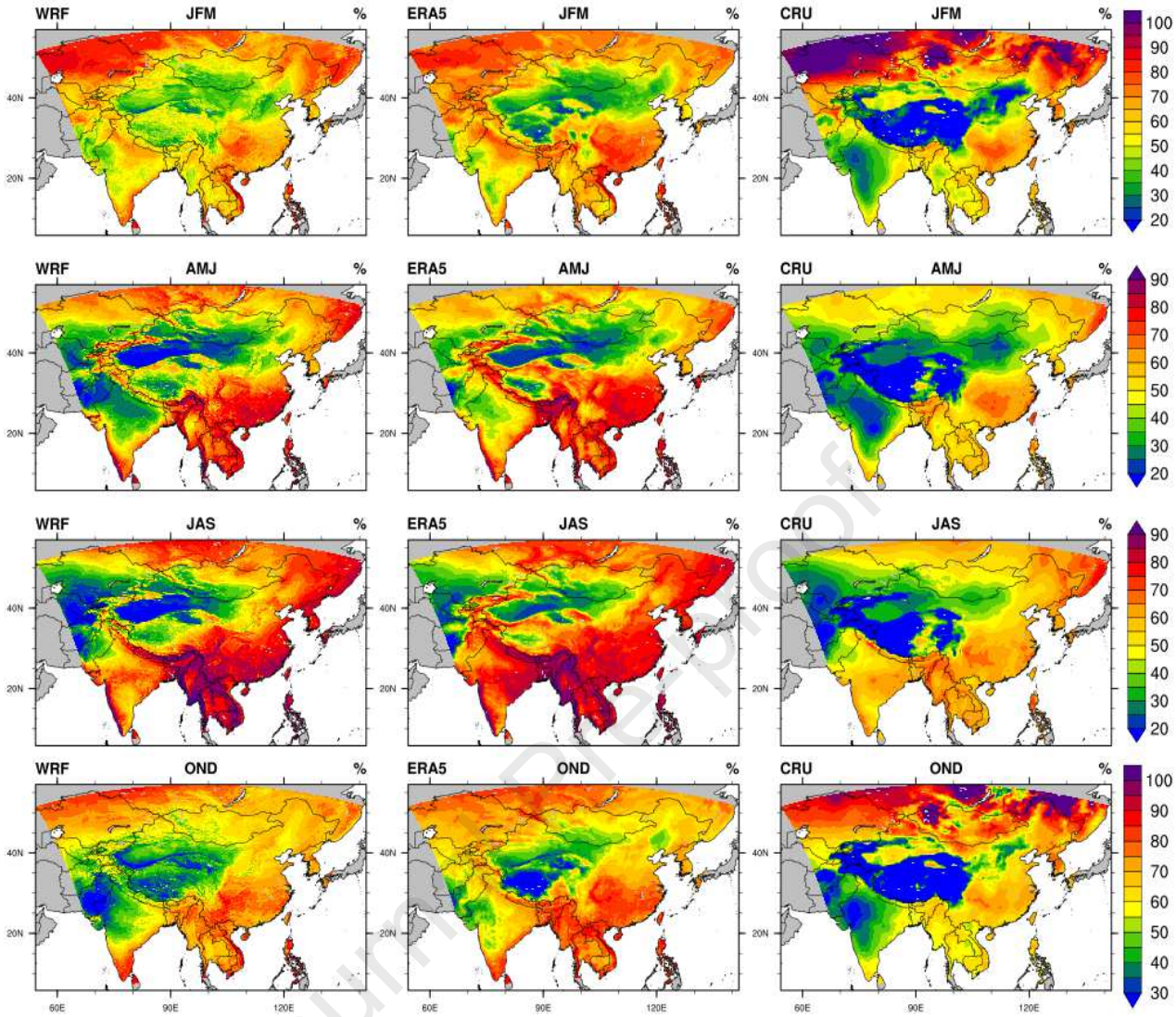

Figure 3. Spatial pattern of 2-meter relative humidity (%) as simulated by WRF-Chem (left panels) and compared to ERA5 reanalysis (central panels) and CRU dataset (right panels) during different seasons (JFM: January-February-March, AMJ: April-May-June, JAS: July-August-September, OND: October-November-December). Mind the differences in color scales between seasonal climatologies.

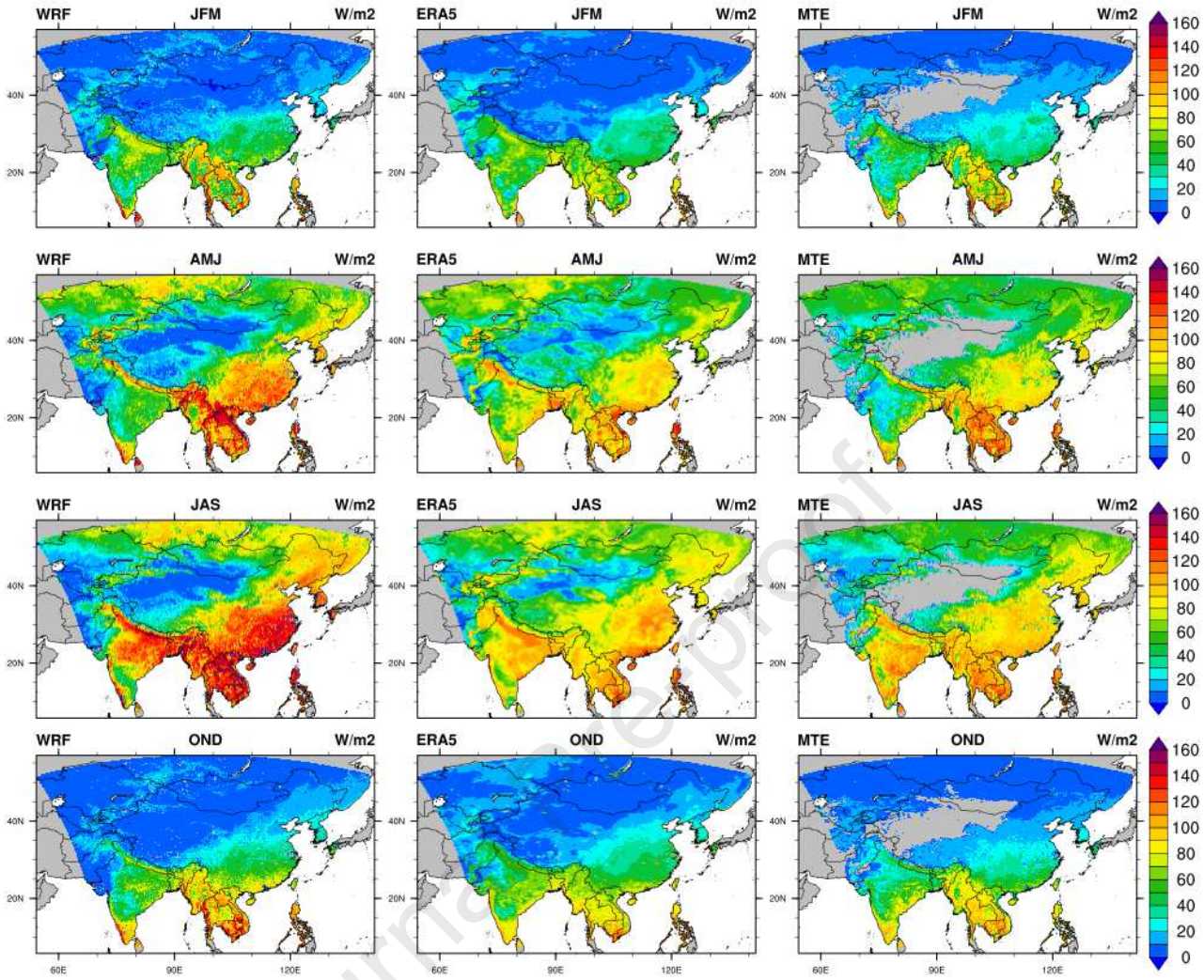

Figure 4. Spatial pattern of surface latent heat (W/m²) as simulated by WRF-Chem (left panels) and compared to ERA5 reanalysis (central panels) and CRU dataset (right panels) during different seasons (JFM: January-February-March, AMJ: April-May-June, JAS: July-August-September, OND: October-November-December).

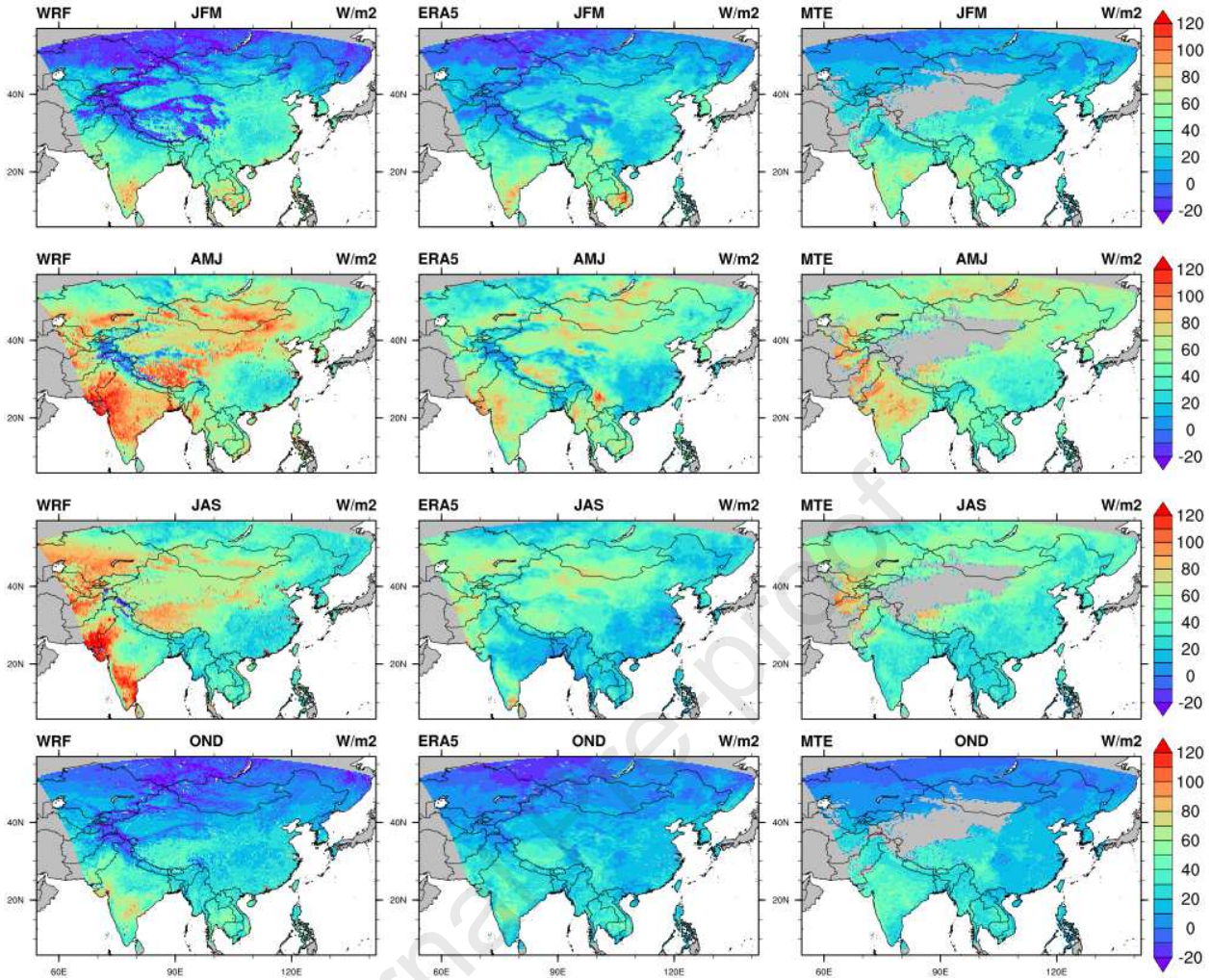

1264

1265 **Figure 5.** Spatial pattern of surface sensible heat (W/m²) as simulated by WRF-Chem (left
1266 panels) and compared to ERA5 reanalysis (central panels) and CRU dataset (right panels)
1267 during different seasons (JFM: January-February-March, AMJ: April-May-June, JAS: July-
1268 August-September, OND: October-November-December).

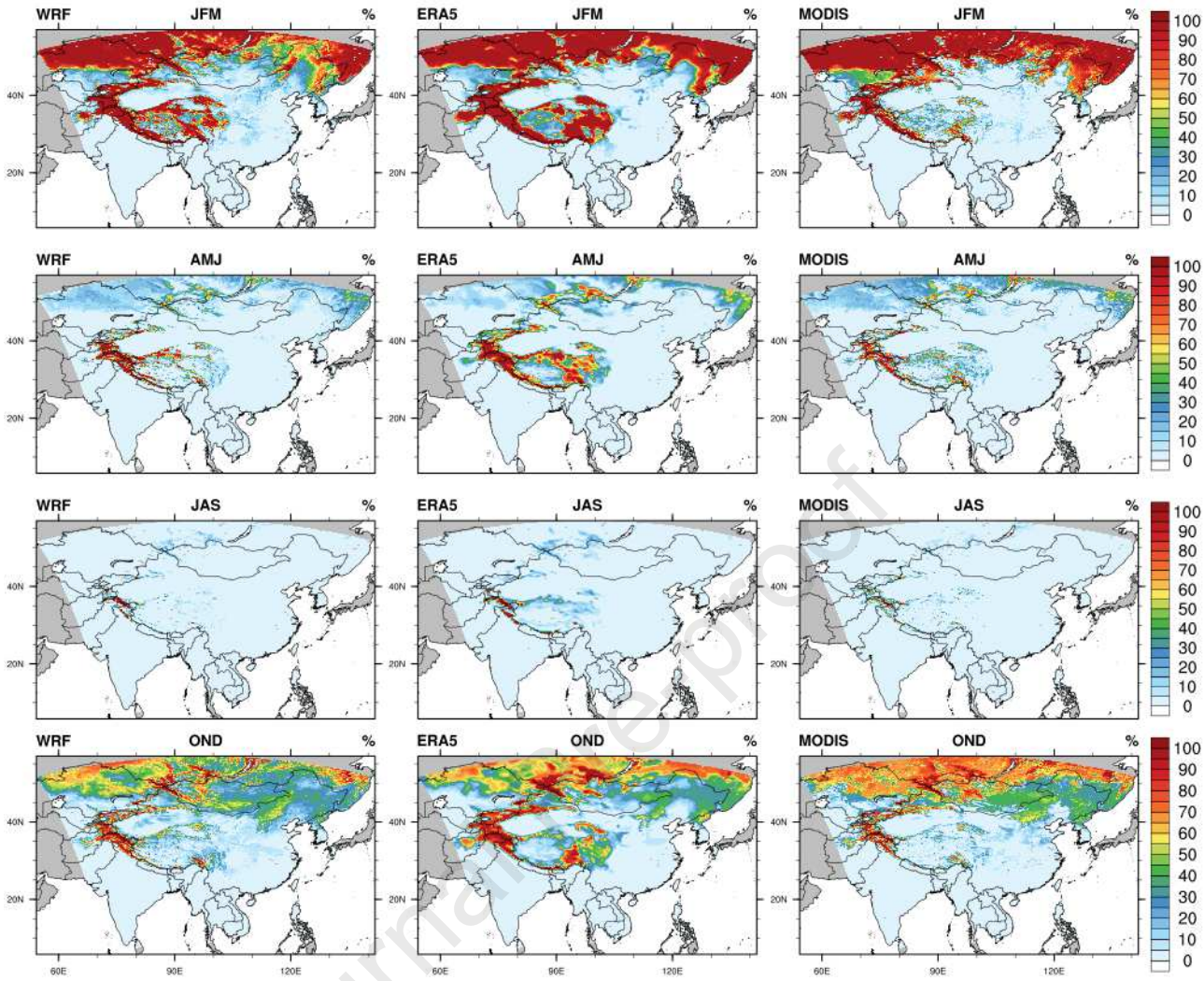

Figure 6. Seasonal spatial pattern of snow fractional cover (%) as simulated by WRF-Chem (left panels) and compared to ERA5 (center panels) and MODIS data (right panels) during different seasons (JFM: January-February-March, AMJ: April-May-June, JAS: July-August-September, OND: October-November-December).

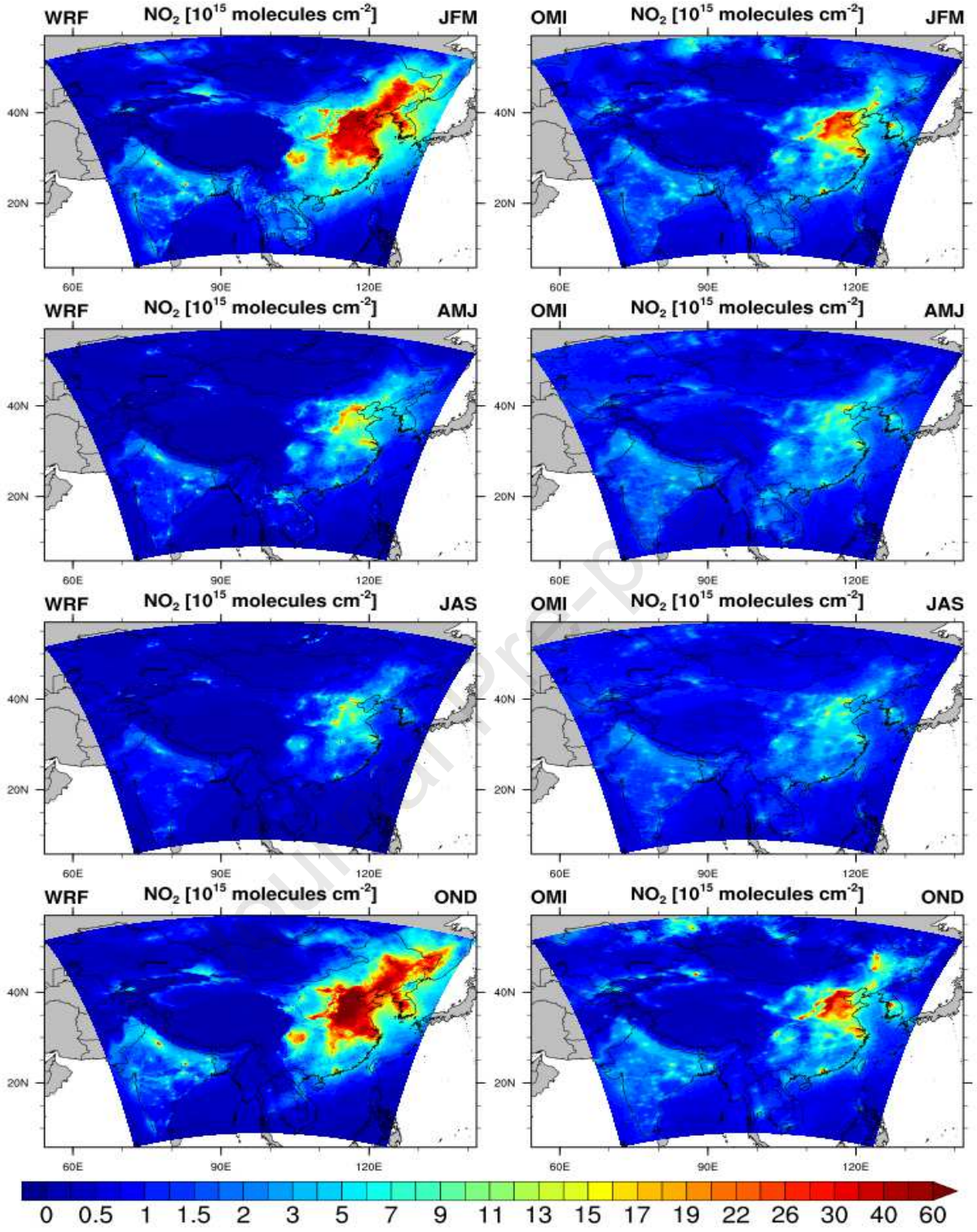

Figure 7. Spatial distributions of WRF-Chem simulated and OMI- retrieved tropospheric NO_2 content (x 10^{15} molecules/cm²) during different seasons (JFM: January-February-March, AMJ: April-May-June, JAS: July-August-September, OND: October-November-December).

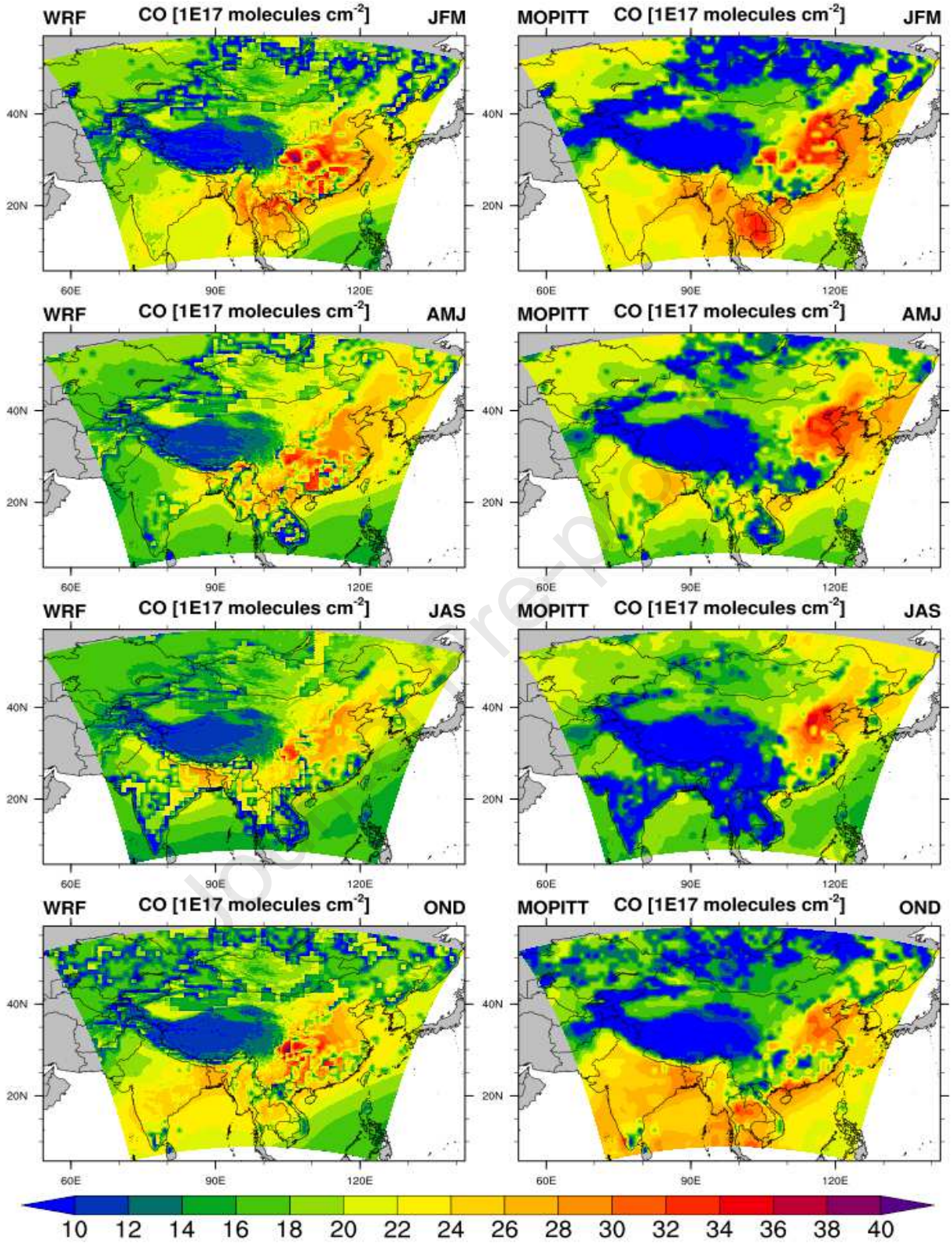

Figure 8. Comparison of WRF-Chem simulated total CO column with MOPITT data (x 10^{17} molecules/cm^2) during different seasons (JFM: January-February-March, AMJ: April-May-June, JAS: July-August-September, OND: October-November-December). The WRF-Chem simulated CO are quite discontinuous due to coarse spatial resolution of MOPITT data (1x1 deg) to compute WRF total column.

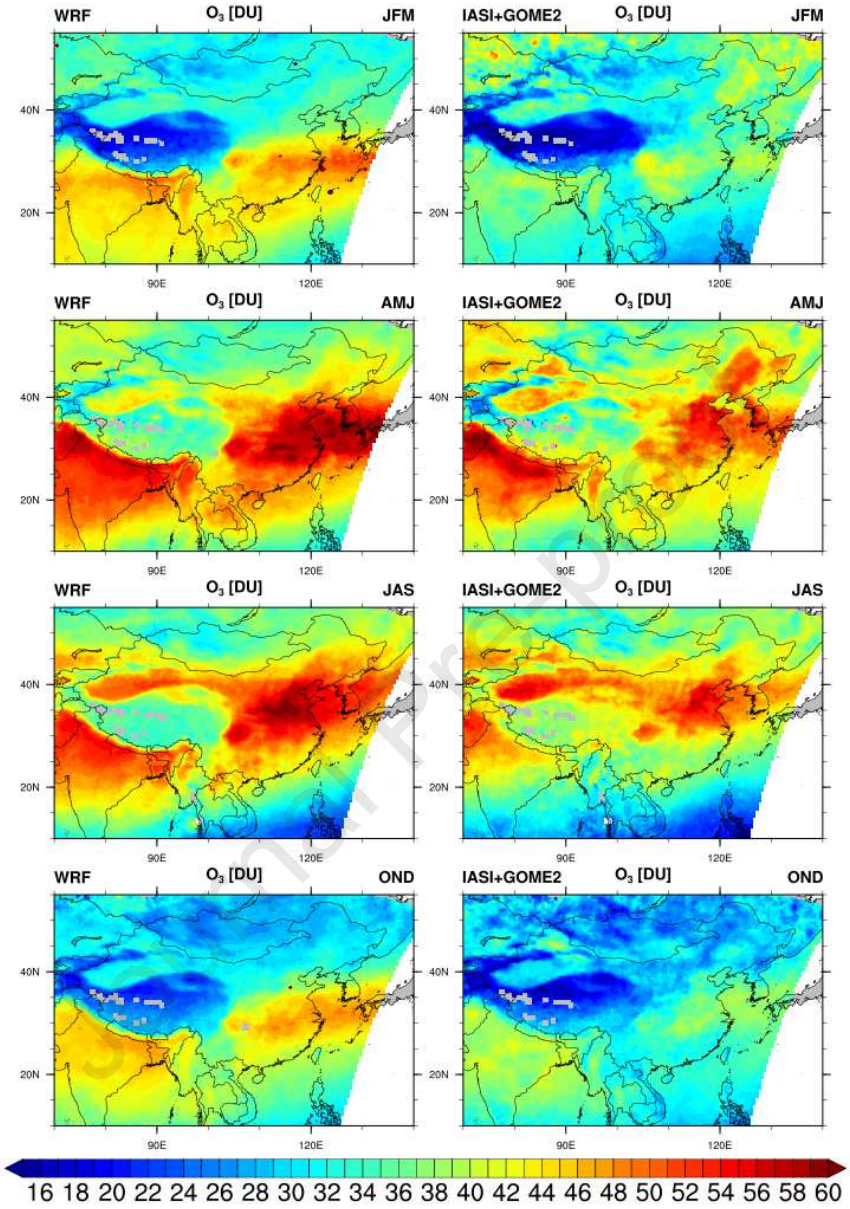

Figure 9. Spatial tropospheric column ozone (Dobson Unit, DU), integrated between the surface and the tropopause, according to the WRF-Chem model (left panels) and IASI-GOME2 satellite retrievals (right panels) during different seasons (JFM: January-February-March, AMJ: April-May-June, JAS: July-August-September, OND: October-November-December).

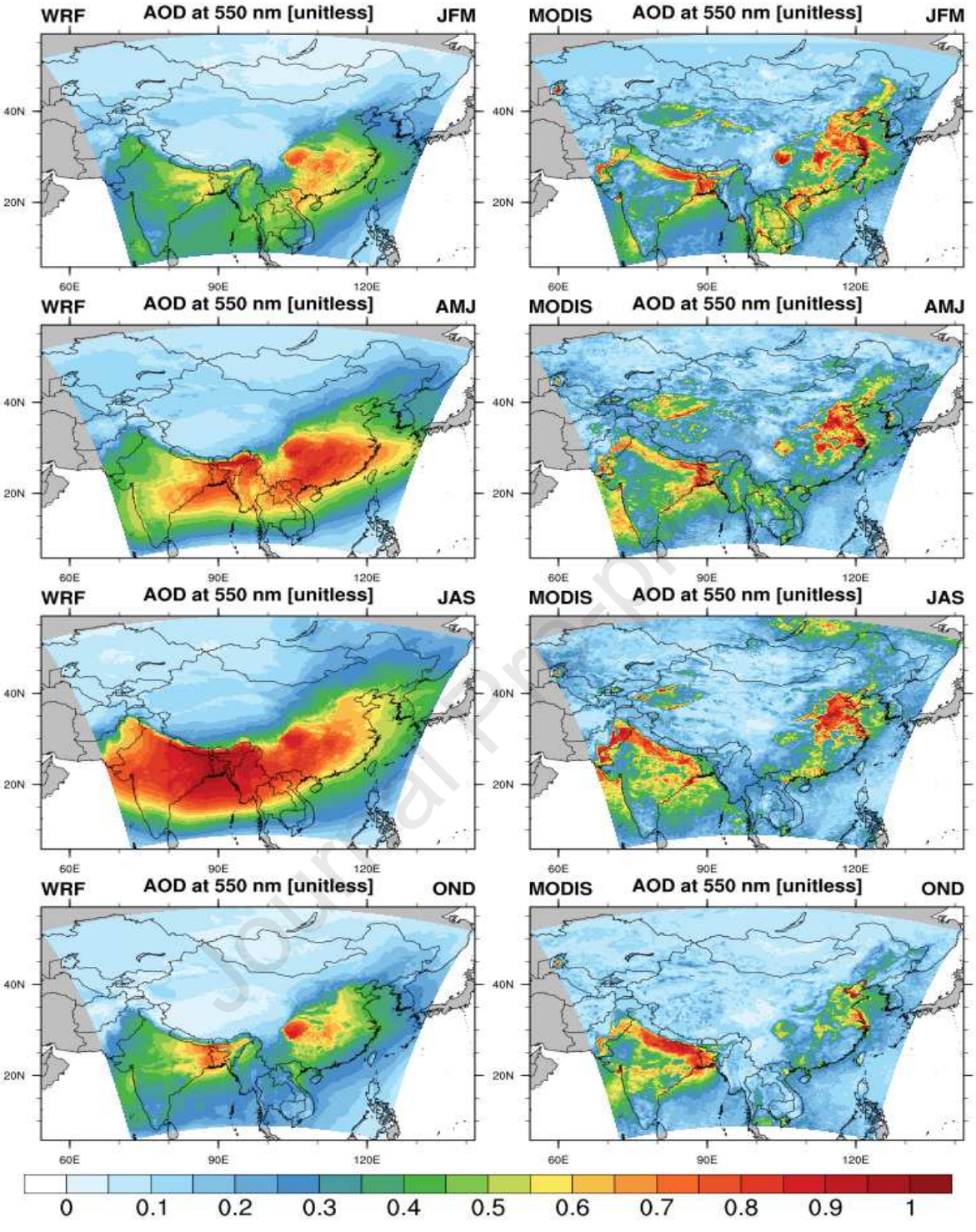

Figure 10. Comparison of simulated aerosol optical depth (dimensionless) with MODIS data during different seasons (JFM: January-February-March, AMJ: April-May-June, JAS: July-August-September, OND: October-November-December).

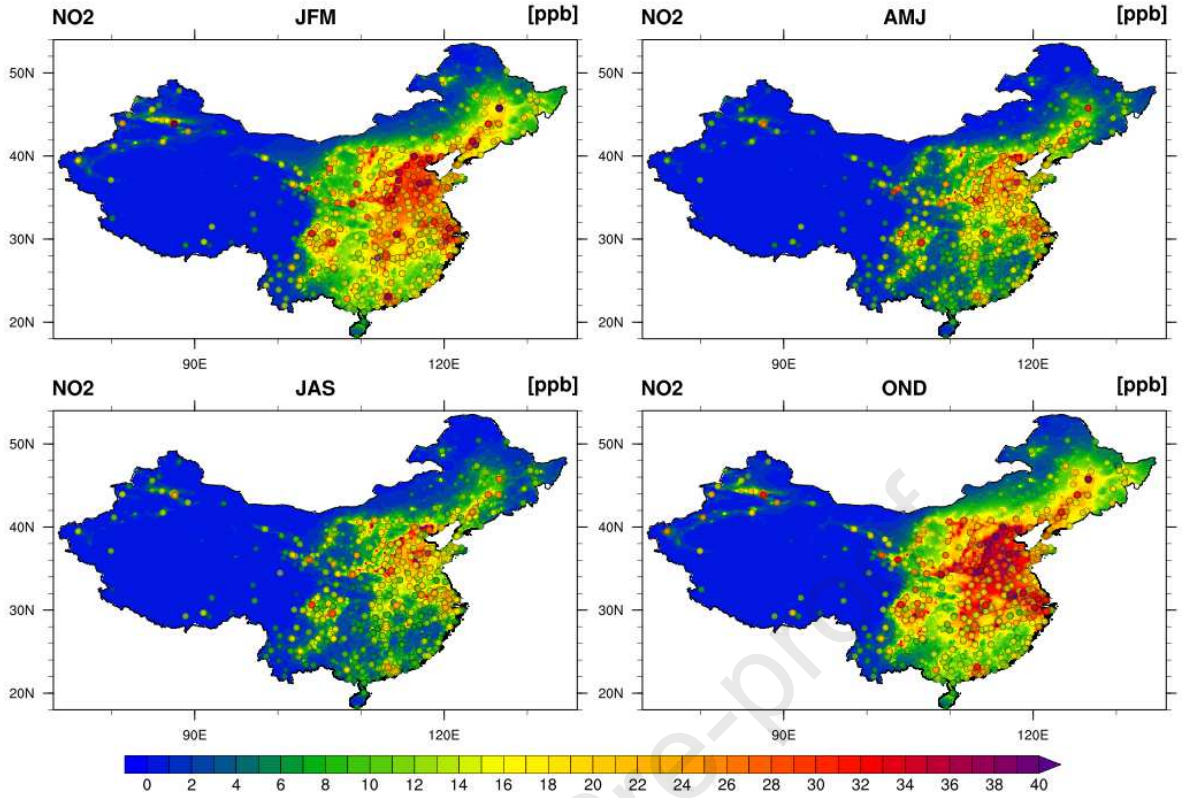

Figure 11. Spatial distributions of surface NO_2 concentrations (in ppb) simulated by the WRF-Chem model (background) and from air quality monitoring stations (dots) across China in 2015 during different seasons (JFM: January-February-March, AMJ: April-May-June, JAS: July-August-September, OND: October-November-December).

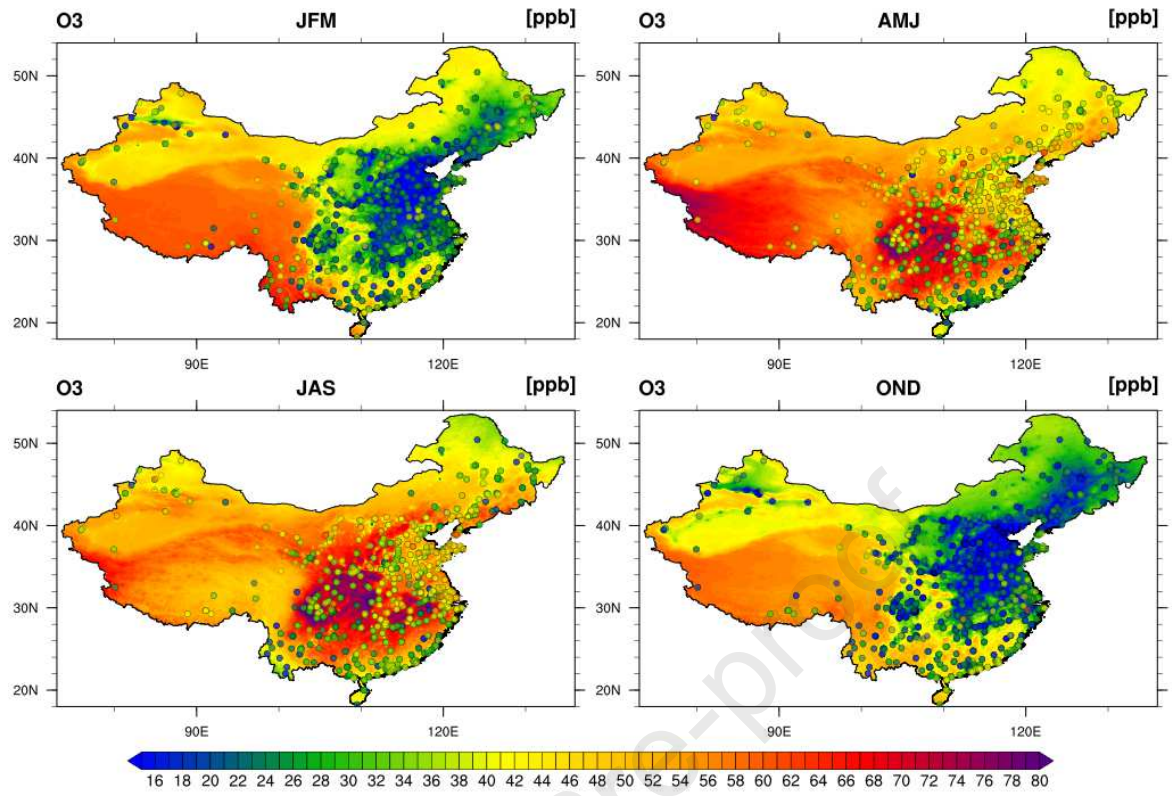

Figure 12. Spatial distributions of surface O_3 concentrations (in ppb) simulated by the WRF-Chem model (background) and from air quality monitoring stations (dots) across China in 2015 during different seasons (JFM: January-February-March, AMJ: April-May-June, JAS: July-August-September, OND: October-November-December).

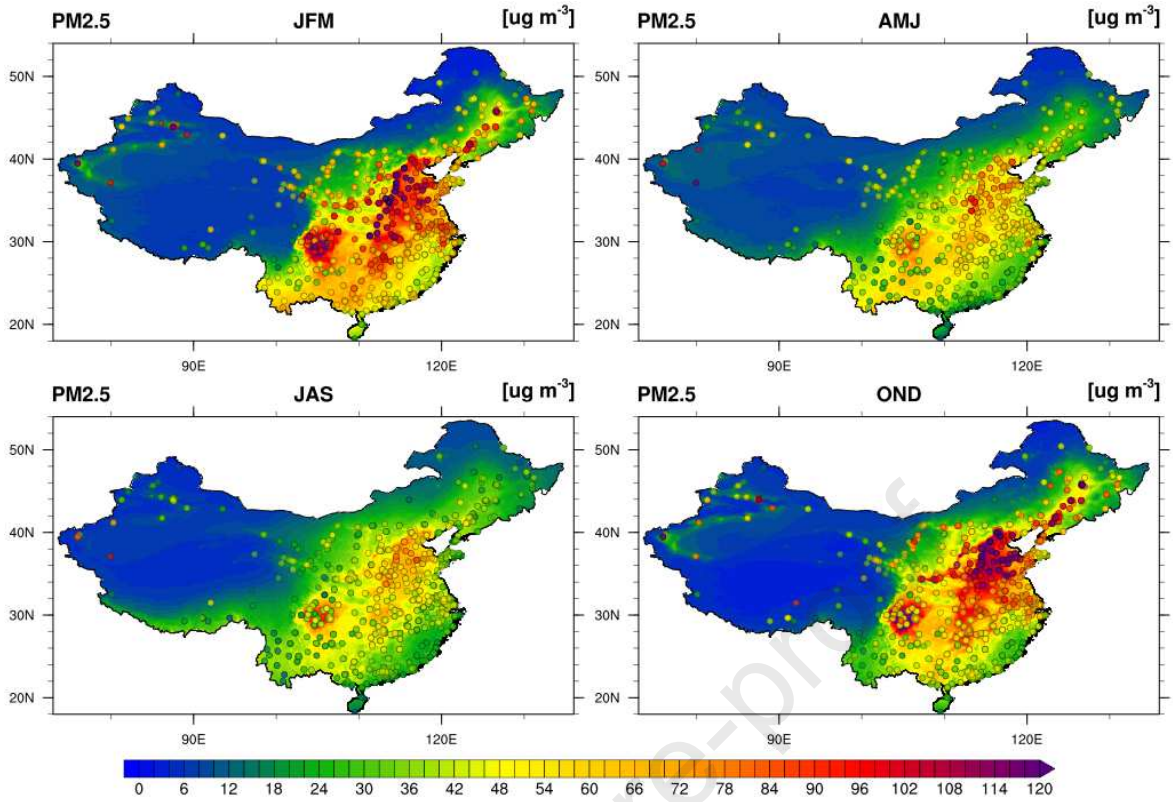

Figure 13. Spatial distributions of surface $PM_{2.5}$ concentrations (in µg m^{-3}) simulated by the WRF-Chem model (background) and from air quality monitoring stations (dots) across China in 2015 during different seasons (JFM: January-February-March, AMJ: April-May-June, JAS: July-August-September, OND: October-November-December).

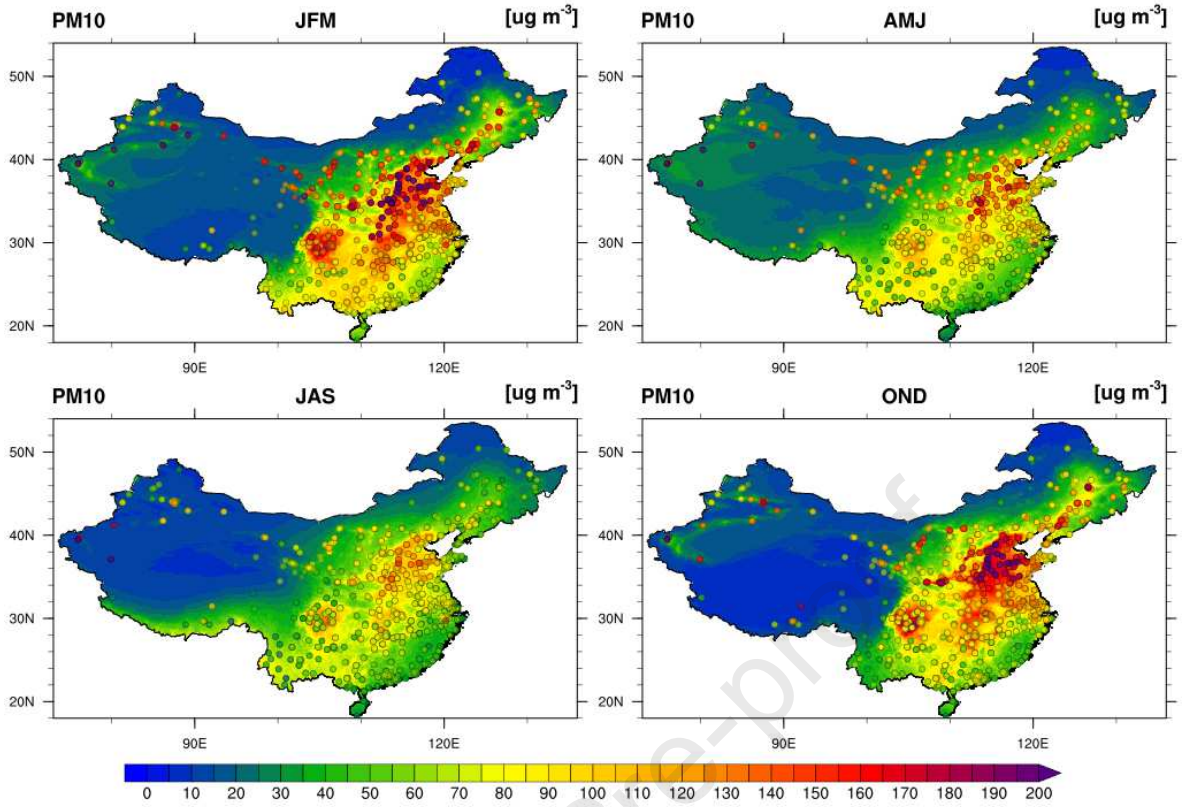

Figure 14. Spatial distributions of surface PM_{10} concentrations (in µg m^{-3}) simulated by the WRF-Chem model (background) and from air quality monitoring stations (dots) across China in 2015 during different seasons (JFM: January-February-March, AMJ: April-May-June, JAS: July-August-September, OND: October-November-December).

Highlights

The WRF-Chem model was applied over Asia in 2015 at 8-km horizontal resolution

The outputs were evaluated against satellite and ground-based observations in China in 2015

WRF-Chem reproduced well the spatio-temporal patterns for meteorological and chemical variables

WRF-Chem reliable tool for air pollution risk assessment to human and ecosystems health

Declaration of interests

☒ The authors declare that they have no known competing financial interests or personal relationships that could have appeared to influence the work reported in this paper.

☐The authors declare the following financial interests/personal relationships which may be considered as potential competing interests: